

discovered from data collected with the *XMM-Newton* (Stelzer et al. 2004; Robrade & Schmitt 2007) and *Chandra X-ray* observatories (Feigelson & Lawson 2004). Several optical and infrared surveys followed by ground-based spectroscopic observations expanded the census of Chamaeleon stars and confirmed the most likely members associated to the molecular clouds (see e.g. Hughes & Hartigan 1992; Prusti et al. 1992; Cambresy et al. 1998; Persi et al. 2000; Vuong et al. 2001; Carpenter et al. 2002; Barrado y Navascués & Jayawardhana 2004; Comerón & Claes 2004; López Martí et al. 2004, 2005; Luhman 2004; Luhman et al. 2004; Allers et al. 2007; Luhman 2007). The most recent census of the stellar population of Cha I is given by Esplin et al. (2017) and contains 250 stars. Analogously, the list of 63 stars studied by Alcalá et al. (2008) and Spezzi et al. (2008) represents the most complete sample of stars in Cha II to date.

The distance to Chamaeleon has undergone extensive revision in recent decades. Early studies reported distance estimates to Cha I in the range from 115 to 215 pc (Grasdalen et al. 1975; Rydgren 1980; Hyland et al. 1982; Schwartz 1992), and suggested that the distance to Cha II could be as large as 400 pc (Fitzgerald et al. 1976; Graham & Hartigan 1988). Franco (1991) investigated the interstellar extinction of field stars projected towards the Chamaeleon clouds and estimated distances of 140 pc and 158 ± 40 pc to Cha I and Cha II, respectively. A subsequent study conducted by Hughes & Hartigan (1992) based on the same technique derived the distance of 200 ± 20 pc to Cha II. In the following years, Whittet et al. (1997) derived the more robust distance estimates of 160 ± 15 pc and 178 ± 18 pc for Cha I and Cha II, respectively, based on multiple distance indicators. Bertout et al. (1999) computed the distance of 168^{+14}_{-12} pc to Cha I from the trigonometric parallaxes delivered by the *Hipparcos* satellite (ESA 1997) for a few stars in this region. A major contribution to the effort in constraining the distance to the Chamaeleon clouds was made by Voirin et al. (2018), where the authors combined the extinction distribution of field stars projected towards the clouds with the parallaxes delivered by the first data release of the *Gaia* space mission (Gaia-DR1, Gaia Collaboration et al. 2016) to estimate the distances of 179^{+11+11}_{-10-10} pc, 181^{+6+11}_{-5-10} pc, 199^{+8+12}_{-7-11} pc to Cha I, Cha II and Cha III, respectively. This study put Cha I about 20 pc further away from previous estimates and returned the first distance determination to the Cha III molecular cloud. However, the systematic uncertainties of 0.3 mas in the Gaia-DR1 parallaxes (Lindgren et al. 2016) largely dominated the distance uncertainties obtained in that study and called for a revision of the results. More recently, Roccatagliata et al. (2018) used the parallaxes from the second data release of the *Gaia* space mission (Gaia-DR2, Gaia Collaboration et al. 2018) to revisit the distance to Cha I. These latter authors reported distances of $192.7^{+0.4}_{-0.4}$ pc and $186.5^{+0.7}_{-0.7}$ pc to the northern and southern subgroups of stars in this cloud, respectively. The improved precision level in the distance determination is related to the more precise parallaxes, but also to the fact that the systematic errors of the Gaia-DR2 catalogue (see e.g. Lindgren et al. 2018; Luri et al. 2018) were not modelled in that solution.

Kinematic studies have proven to be fundamental in distinguishing between the different subgroups of the Chamaeleon region and to searching for new cluster members. For example, Lopez Martí et al. (2013) found evidence that the stars in Cha I and Cha II have different proper motions, and that they also differ from the adjacent ϵ Cha and η Cha associations that populate the same region of the sky. In a subsequent study, López Martí et al. (2013) identified new kinematic members in Cha I and Cha II located in the outskirts of the molecular clouds and

argued that this dispersed population could be larger, but more accurate data would be required to confirm this hypothesis. Indeed, the scarcity of trigonometric parallaxes and radial velocity (RV) information for most stars in Chamaeleon has been the main limitation to studying the kinematic properties of this region. This situation has dramatically changed with the advent of the Gaia-DR2 catalogue combined with the spectroscopic observations conducted by the *Gaia*-ESO Survey (Gilmore et al. 2012) in the Chamaeleon region (see e.g. Sacco et al. 2017). Altogether, this puts us in a timely position to investigate the 3D structure and 3D space motion of the Chamaeleon star-forming complex with unprecedented precision as discussed throughout this study.

This paper is one in a series conducted in the context of the Dynamical Analysis of Nearby Clusters project (DANCe, Bouy et al. 2013). Here, we investigate the census of stars, and the structure and kinematic properties of the Chamaeleon star-forming region in light of Gaia-DR2 data. The paper is organised as follows. In Section 2 we compile the lists of stars in Cha I and Cha II published in the literature, and perform a new membership analysis to confirm the historical members associated with these clouds and discover new ones. In Section 3 we revisit the distance, spatial velocity, and age of the Chamaeleon subgroups based on our new sample of cluster members selected in this study. Finally, we summarise our results and conclusions in Section 4.

2. Membership analysis

Our strategy to assess membership is based on the methodology previously developed by our team (Sarro et al. 2014; Olivares et al. 2019). In this section, we describe the main steps of our membership analysis applied to the Chamaeleon star-forming region and we refer the reader to the original papers for more details on the performance and implementation of our classifier.

2.1. Field and cluster models

The representation space (i.e., set of observables) that we use in the membership analysis includes the astrometric and photometric features of the stars provided in the Gaia-DR2 catalogue. We do not include the blue photometry G_{BP} in the analysis because of the calibration problems in this band as reported in the literature (see e.g. Maíz Apellániz & Weiler 2018) which can affect our selection of cluster members particularly in the faint end. We therefore restrict the membership analysis to the space of observables defined by $\mu_\alpha \cos \delta$, μ_δ , ϖ , G_{RP} and $G - G_{RP}$. We then downloaded the Gaia-DR2 catalogue in the region of the sky defined by $295^\circ \leq l \leq 305^\circ$ and $-20^\circ \leq b \leq -10^\circ$ in Galactic coordinates which encompasses the three molecular clouds of the complex (Cha I, Cha II, and Cha III). This field includes 4 433 409 sources and 3 904 492 of them have complete data in our representation space.

The field population was modelled using Gaussian Mixture Models (GMMs). We tested the field model with a random sample of 10^6 sources using GMMs with 20, 40, 60, 80, 100, 120, 140 and 160 components, and we chose the model with 80 components, which returns the smallest Bayesian information criteria (BIC) value. The field model was computed only once at the beginning while the cluster model was built iteratively during the process based on an initial list of members (see below). The cluster model uses the inferred parameters from the initial list of members to define the cluster locus in the space of the astrometric features using GMMs and defines the cluster sequence in the

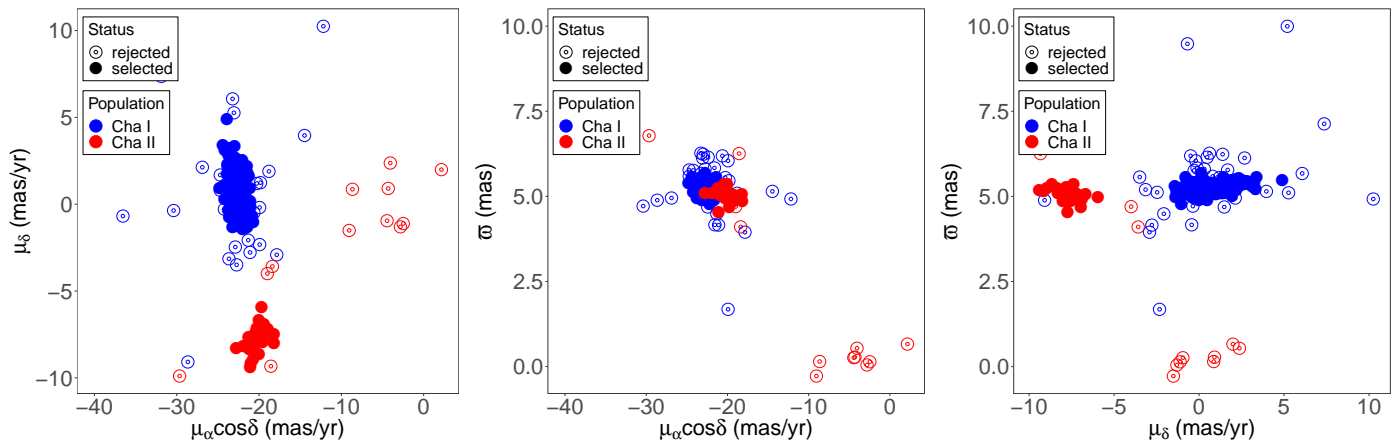


Fig. 1. Proper motions and parallaxes of the stars in Cha I and Cha II in the samples of [Esplin et al. \(2017\)](#) and [Alcalá et al. \(2008\)](#), respectively. Open symbols denote potential outliers in these samples based on Gaia-DR2 data identified from the MCD estimator (see Sect. 2).

photometric space as a principal curve with a spread at any point along the curve given by a multivariate Gaussian (both the principal curve and its spread are initialised with a fit to the initial list of members). The method then computes membership probabilities for all sources in the field using the fraction of sources in each category (member vs. non-member) obtained in the previous iteration to estimate the marginal class probabilities. The sources are classified into members and non-members based on a probability threshold p_{in} predefined by the user. The list of stars that results from this process is used as input for the next iteration and this procedure is repeated until convergence. The solution is said to converge when the list of cluster members remains fixed after successive iterations.

The final step of the membership analysis consists in evaluating the performance of our classifier. We generate synthetic data based on the cluster and field properties inferred from the previous steps, and measure the quality of the classifier to define an optimum probability threshold p_{opt} as described in Sect. 4.2.7 of [Olivares et al. \(2019\)](#). The sources in the catalogue are finally re-classified as members ($p \geq p_{opt}$) and non-members.

The samples of 250 stars from [Esplin et al. \(2017\)](#) and 63 stars from [Alcalá et al. \(2008\)](#) represent the most complete censuses of the stellar population in Cha I and Cha II, respectively, known to date. We found Gaia-DR2 astrometry for 194 and 48 stars, respectively, where we note the existence of a few stars with discrepant proper motion and parallax in these samples as shown in Figure 1. We computed robust distances based on the covariance matrix obtained from the minimum covariance determinant (MCD, [Rousseeuw & Driessen 1999](#)) estimator and removed potential outliers from these samples as described in Section 2.1 of [Galli et al. \(2020a\)](#). This step reduces the lists of stars (with Gaia-DR2 data) in Cha I and Cha II to 161 and 36 stars, respectively. We use these clean samples of stars as the initial list of members in our membership analysis. The stars in Cha I and Cha II exhibit distinct properties as discussed throughout this paper (see also Figure 1) despite them being part of the same molecular cloud complex. We therefore decided to run two independent membership analyses (one for each cluster) using the same catalogue of Gaia-DR2 sources downloaded for this sky region, representation space, and strategy to select the most likely cluster members, as described above, but using different input lists of stars that are specific for each case.

In Table 1 we compare the solutions obtained for Cha I and Cha II using different values of the user predefined probability threshold p_{in} . We compute the true positive rate (TPR, i.e. the fraction of synthetic cluster members recovered by our methodology) and contamination rate (CR, i.e. the fraction of synthetic field stars identified by our model as cluster members) of the classifier to better evaluate our results obtained with different p_{in} values. These numbers were obtained from synthetic data sets sampled from the inferred model for each cluster, and so they represent only rough estimates of these indicators computed in the absence of the true distributions.

2.2. Projection effects

Our membership analysis conducted over the relatively large field that encompasses the Chamaeleon molecular clouds (as defined in Sect. 2.1) identifies a few more dispersed field sources as cluster members independent of the adopted p_{in} threshold. In particular, we note the existence of one source (namely Gaia DR2 5789232155389250304) that is closer to the Cha II molecular clouds, but exhibits proper motion and parallax that are consistent with membership in Cha I. The RV of this source published in the literature yields a spatial velocity ($U = -11.0 \pm 1.5$ km/s, $V = -21.6 \pm 2.0$ km/s, $W = -1.8 \pm 0.6$ km/s) that is not consistent with the space motion of Cha I stars (see Sect. 3.3). This is due to projection effects that render proper motion and parallax consistent with membership in Cha I at the spatial location of this source despite the different space motion. We proceed as follows to minimise the existence of potential contaminants in our solution due to projection effects.

First, we conduct an independent membership analysis following the same methodology described before but in two smaller regions centred around the Cha I and Cha II molecular clouds. Our results obtained in these regions are labelled with the term ‘central region’ which we use hereafter to distinguish from the membership analysis conducted over the entire Chamaeleon complex. The size of each field is defined based on the position of the candidate members previously identified in the literature with available Gaia-DR2 data that constitute our input list for the membership analysis (see Sect. 2.1). Thus, the field for the membership analysis in Cha I covers the sky region defined by $295.9^\circ \leq l \leq 297.8^\circ$, $-16.1^\circ \leq b \leq -13.1^\circ$ in Galactic coordinates and includes 196 330 sources. The field centred around

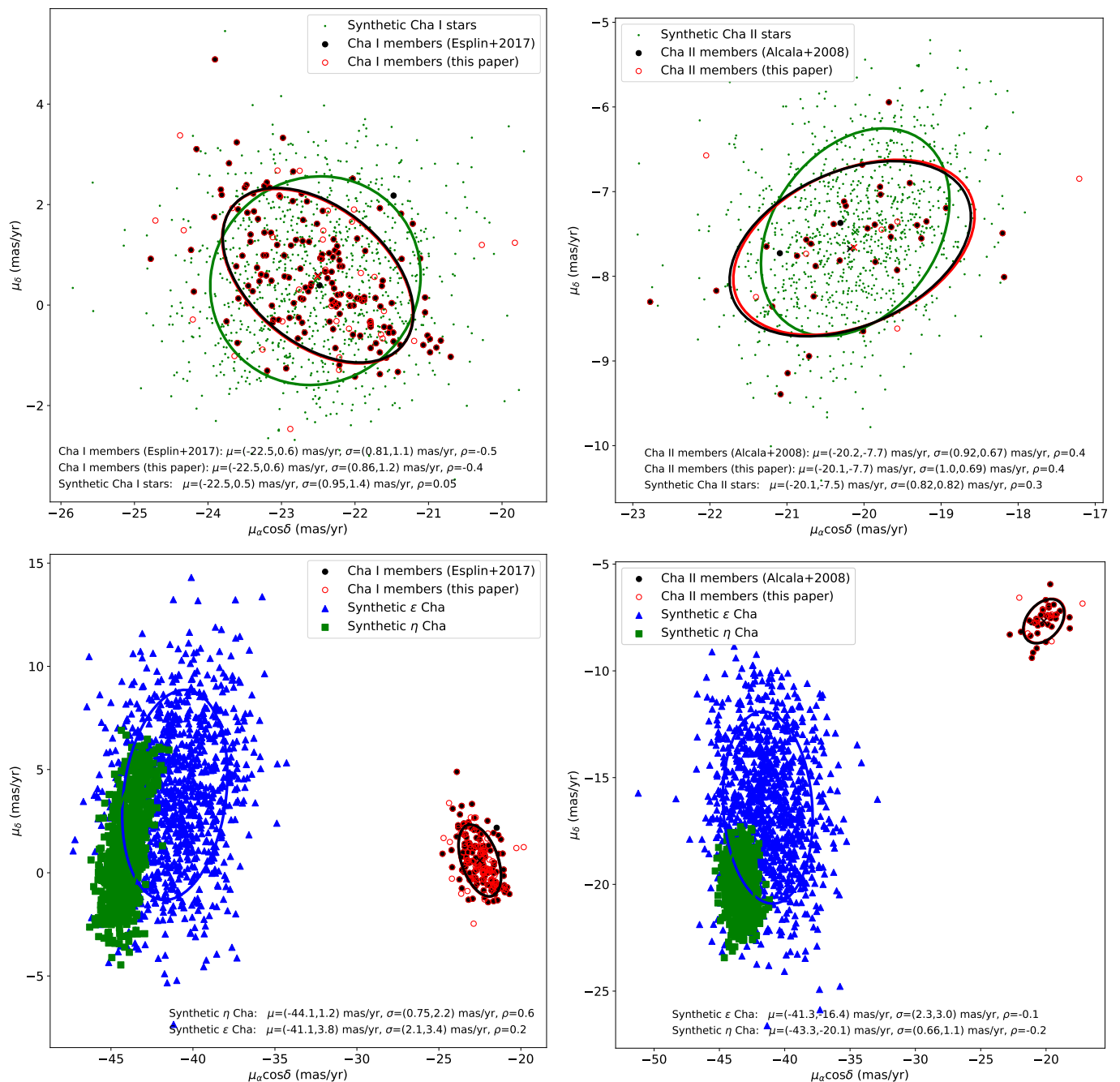


Fig. 2. Projection effects on the stellar proper motion of Chamaeleon stars. Upper panels show the proper motion distribution of synthetic stars randomly distributed over the fields used in our membership analysis moving with the same space motion of Cha I and Cha II stars. Lower panels illustrate the expected proper motion distribution of synthetic ϵ Cha and η Cha located in the same fields. We generated a total of 1 000 sources in our simulations. We compare the proper motion of the synthetic stars with the observed values for the candidate members previously identified in the literature and members identified in this study (in this case we use the solution with $p_{in} = 0.9$, see Table 1). The mean, dispersion and correlation coefficient obtained from each proper motion distribution are indicated in the panels. The solid lines denote the fitted proper motion distributions and the crosses mark the mean proper motion in each case.

Cha II is defined by $303.2^{\circ} \leq l \leq 304.2^{\circ}$, $-15.1^{\circ} \leq b \leq -13.6^{\circ}$ and includes 56 100 sources.

Second, we generated synthetic cluster members located in the fields surveyed by our membership analysis from the velocity and distance distribution of the Cha I and Cha II candidate members previously identified in the literature. The 3D positions and spatial velocities of the stars were transformed into the observable proper motions in the corresponding sky regions that we use

to discuss the importance of projection effects in our analysis. As illustrated in Figure 2 the location and scatter of the proper motion distribution for synthetic stars, candidate members from the literature, and members identified in this study are consistent between themselves. The orientation of the proper motion distribution generated in our simulations is different because we allow the synthetic cluster members to be randomly distributed in the fields covered by our membership analysis. This effect

is more apparent in the case of Cha I. Therefore, our methodology employed for the membership analysis could be missing some cluster members if we assume that the stars are equally probable to be found at any sky position of the field. However, what we observe in practice is that the true members are mostly projected towards the molecular clouds (and in their immediate vicinity) which explains the different orientation observed for the simulated proper motions. The proper motion distribution of the members identified in this study is in good agreement with the results given in the literature. This confirms that our results for the membership analysis in the central regions are not affected by projection effects.

Third, we performed additional simulations to investigate the existence of contaminants from other young stellar groups due to projection effects. As described in Sect. 2.1, our membership analysis uses not only the astrometric features of the stars, but also their photometry to select cluster members with similar ages. The only two young stellar groups in the Chamaeleon complex that have similar ages to the stellar populations in the molecular clouds are the ϵ Cha and η Cha associations. We generated synthetic stars (as described above) using the distance and space motion of these stellar groups given in the literature (see e.g. Murphy et al. 2013) in the fields covered by our membership analysis of Cha I and Cha II. Figure 2 shows that the proper motions of the synthetic ϵ Cha and η Cha stars are significantly different from the observed proper motion distribution of Cha I and Cha II cluster members. We therefore conclude that our sample of members in the central regions is not contaminated by the other young stellar groups of the Chamaeleon complex due to projection effects.

2.3. Final list of cluster members

The high TPRs and low CRs for all solutions given in Table 1 confirm the robustness of our results. In particular, we note that our results for the membership analysis in the central regions have higher TPRs and lower CRs as compared to the ones obtained over the whole Chamaeleon complex. We see little variation in sample size in the two cases and confirm that running the membership analysis over extended regions of the Chamaeleon complex will not allow us to detect more cluster members (but will lead to the inclusion of more contaminants due to projection effects). On the contrary, performing the membership analysis over smaller regions allowed us to recover a few members that have been overlooked in the first analysis. We therefore decided to report the solutions obtained with $p_{in} = 0.9$ in the central regions as our final lists of clusters members in Cha I (188 stars) and Cha II (41 stars). The cluster members in each population are listed in Tables A.1 and A.2. We provide in Tables A.3 and A.4 the membership probabilities obtained with different p_{in} values for all sources in the field for the analyses conducted in Cha I and Cha II, respectively, to allow the reader to choose a different probability threshold that is more suited to their study.

Figure 3 confirms the existence of a more dispersed population of cluster members in the immediate vicinity of the Cha I molecular cloud that is known from pre-*Gaia* studies (see e.g. López Martí et al. 2013). Figures 4 and 5 show the distribution of proper motions and parallaxes of the Cha I and Cha II members identified in our analysis. As expected, the cluster members in the outskirts of the distributions and with the largest uncertainties have the lowest membership probabilities. The colour-magnitude diagrams of Cha I and Cha II in the chosen photometric space are shown in Figure 6, and the empirical isochrones are given in Tables A.5 and A.6. Our samples of cluster members

cover the magnitude range from about $G = 6$ to $G = 20$ mag and $G = 12$ to $G = 18$ mag in Cha I and Cha II, respectively, and they represent the most complete censuses of members in the Chamaeleon clouds (with available astrometry in the Gaia-DR2 catalogue) to date.

In Figure 7 we compare the samples of cluster members identified in this paper with the lists of Cha I and Cha II stars (with available Gaia-DR2 data) published in other studies. We note that most members in the Cha I sample (i.e., 169 stars) were also included in the study conducted by Esplin et al. (2017). However, 25 sources presented in that study could not be recovered by our membership analysis. We verified that they have proper motions and parallaxes that are either not consistent with membership in Cha I (see e.g. Figure 1) or result from poor astrometric solutions. For example, if we use the re-normalised unit weight error (RUWE) criterion¹ to filter the literature sources with poor astrometry (see Sect. 3.1) we note that 17 stars among the rejected sources fail to pass this selection criterion (i.e. $\text{RUWE} < 1.4$). These 17 sources can be considered at this stage as potential candidate members and future data releases of the Gaia space mission will allow us to confirm (or exclude) membership with more precise data. Three stars among the other eight rejected candidate members from the literature lie outside the region surveyed by our analysis. Only one rejected star from the literature among the remaining five sources (namely, Gaia DR2 5201125062389375872) has proper motions and parallaxes consistent with membership in Cha I. However, it is located below the empirical isochrone of the cluster which explains why it is rejected by our methodology. The same conclusion holds if we try to correct its photometry by the effect of interstellar extinction using the value of $A_V \approx 2.5$ mag that is estimated from the Dobashi et al. (2005) maps at the location of the source.

Similar arguments apply to the analysis in Cha II. We confirmed 34 members from Alcalá et al. (2008) and rejected 14 stars from that study. We note that among the rejected members there are eight sources that are more likely to be background objects ($\varpi < 1$ mas) unrelated to the Cha II population (see Figure 1). Four stars have poor astrometric solutions based on the RUWE criterion which could possibly explain the discrepant proper motions and parallaxes. The remaining two stars among the other rejected sources, namely Gaia DR2 5788884464898536960 and Gaia DR2 5788200298087320320, have proper motions and parallaxes consistent with membership in Cha II, but they lie below the empirical isochrone defined by the other cluster members. We tentatively corrected their photometry from the interstellar extinction estimated at their position from the Dobashi et al. (2005) extinction maps, but this correction does not place them on the empirical isochrone of the cluster.

The membership analysis conducted in this study allowed us to identify 19 and 7 new members of Cha I and Cha II, respectively. This represents an increase of about 11% and 21% in the stellar population of Cha I and Cha II with respect to the number of confirmed cluster members from previous studies.

3. Discussion

3.1. Refining the sample of cluster members

Let us now refine our sample of cluster members by filtering the stars with the best data available before deriving the overall kinematic properties of the Chamaeleon subgroups. To do so, we use

¹ see technical note GAIA-C3-TN-LU-LL-124-01 for more details

Table 1. Comparison of membership results in Cha I and Cha II using different values for the probability threshold p_{in} .

Cha I (large field)					Cha II (large field)				
p_{in}	p_{opt}	Members	TPR	CR	p_{opt}	Members	TPR	CR	
0.5	0.80	189	0.964 ± 0.010	0.040 ± 0.017	0.74	48	0.978 ± 0.018	0.039 ± 0.004	
0.6	0.90	183	0.947 ± 0.005	0.024 ± 0.011	0.78	47	0.982 ± 0.013	0.030 ± 0.005	
0.7	0.80	189	0.962 ± 0.014	0.052 ± 0.024	0.59	47	0.977 ± 0.006	0.030 ± 0.016	
0.8	0.84	184	0.972 ± 0.006	0.037 ± 0.016	0.83	40	0.970 ± 0.023	0.030 ± 0.005	
0.9	0.81	187	0.972 ± 0.020	0.034 ± 0.011	0.81	38	0.983 ± 0.010	0.021 ± 0.011	
Cha I (central region)					Cha II (central region)				
p_{in}	p_{opt}	Members	TPR	CR	p_{opt}	Members	TPR	CR	
0.5	0.80	192	0.995 ± 0.005	0.021 ± 0.013	0.74	43	0.980 ± 0.017	0.022 ± 0.003	
0.6	0.84	191	0.996 ± 0.003	0.014 ± 0.008	0.77	41	0.988 ± 0.006	0.012 ± 0.003	
0.7	0.69	192	0.998 ± 0.003	0.012 ± 0.003	0.76	41	0.985 ± 0.013	0.008 ± 0.008	
0.8	0.86	190	0.993 ± 0.008	0.007 ± 0.012	0.78	41	0.983 ± 0.016	0.008 ± 0.003	
0.9	0.90	188	0.991 ± 0.008	0.002 ± 0.003	0.79	41	0.985 ± 0.010	0.017 ± 0.011	

Notes. We provide the optimum probability threshold, the number of cluster members, the true positive rate (TPR) and contamination rate (CR) obtained for each solution and cluster. We present the results of our membership analysis performed over a large field that encompasses the entire Chamaeleon complex (see Sect. 2.1) and the central regions around the Cha I and Cha II molecular clouds (see Sect. 2.2).

the RUWE criterion as one possible indicator of the goodness of fit of the Gaia-DR2 astrometric solution. The value of 1.4 is often used in the literature to distinguish between the sources with reliable (i.e., $\text{RUWE} < 1.4$) and poor astrometric solutions in the Gaia-DR2 catalogue, but some studies adopt different thresholds (see e.g. Luhman & Esplin 2020). In this paper we adopt the RUWE threshold of 1.4 to select the sources with good astrometric solutions for consistency with the methodology adopted in other papers of this series (see e.g. Galli et al. 2020a,b). This step reduces the samples of members to 160 and 31 stars in Cha I and Cha II, respectively. The rejected stars exhibit mostly the largest uncertainties in proper motions and parallaxes as shown in Figures 4 and 5. Many of them have been identified as binaries or multiple systems in the literature (see also Figure 6) which explains the poor astrometry in the Gaia-DR2 catalogue. Future data releases of the Gaia space mission will deliver an improved astrometry for such systems.

We searched the CDS databases (Wenger et al. 2000) for RV information of the stars in our sample. Our search for RVs in the literature is based on Dubath et al. (1996), Covino et al. (1997), Joergens & Guenther (2001), Torres et al. (2006), James et al. (2006), Gontcharov (2006), Guenther et al. (2007), Nguyen et al. (2012), Biazzo et al. (2012), Sacco et al. (2017), and the Gaia-DR2 catalogue. We found RV measurements for 82 and 19 stars in our samples of cluster members in Cha I and Cha II, respectively. Some stars have multiple RV measurements in the literature (collected from different studies) and in such cases we decided to use the most precise value in our analysis.

We applied the interquartile range (IQR) criterion to identify the stars with discrepant RVs in the sample. This method rejects outliers that lie over $1.5 \times \text{IQR}$ below the first quartile or above the third quartile. Doing so, we found four stars in Cha I with discrepant RVs as illustrated in Figure 8. We discarded these RV measurements from the analysis presented below, but we still retain the stars in the sample of cluster members. Their proper motions and parallaxes are consistent with membership in Cha I and the corresponding RVs are more likely to be affected by other reasons (e.g. undetected binaries). This reduces the sample of sources in Cha I with available RV information to 78 stars. We do not discard any RV measurement in the Cha II sample based on the IQR criterion.

Our search for published RV data for Chamaeleon stars in the literature allowed us to retrieve this information for about 49% and 61% of the stars in Cha I and Cha II, respectively. The main source of RV data in Cha I is the study conducted by Sacco et al. (2017) as part of the Gaia-ESO survey, and we therefore refer the reader to that paper for further details on these measurements. In the case of the Cha II molecular cloud, the main source of RV data is the study conducted by Biazzo et al. (2012). The mean precision of the RVs in our sample is 0.5 km/s and 4.7 km/s in Cha I and Cha II, respectively. In the following, we use the precise Gaia-DR2 astrometry combined with published RV data to investigate the distance and spatial velocity of Chamaeleon stars.

3.2. Proper motions and parallaxes of the subgroups

The stellar population of Cha I is composed of two subclusters that have been historically separated based on their position in the sky using the declination of $\delta = -77^\circ$ as midpoint to separate the northern and southern subgroups (see e.g. Luhman 2007). However, a recent study conducted by Roccatagliata et al. (2018) shows that the subclusters overlap and that they cannot be strictly divided by their sky positions.

In this paper, we apply the Partitioning Around Medoids (PAM, Kaufmann & Rousseeuw 1987) clustering algorithm to separate the two subclusters in Cha I. The PAM algorithm is an unsupervised machine-learning method for partitioning a N -dimensional dataset into k groups (i.e. clusters) that works similarly to the k -Means algorithm (MacQueen 1967), but uses medoids to represent the centers of the clusters. We perform the clustering in the 5D space of astrometric observables ($\alpha, \delta, \mu_\alpha \cos \delta, \mu_\delta, \varpi$) of the stars using the *pam* routine from the *cluster* package implemented in R programming language. We use the Average Silhouette (Rousseeuw 1987) and Gap Statistic (Tibshirani et al. 2001) methods to confirm that the optimal number of clusters for our dataset is indeed $k = 2$, which we use as input for the clustering analysis. The clustering analysis with PAM divides the sample into 76 stars and 84 stars for Cha I (north) and Cha I (south), respectively. Figure 9 confirms that the subclusters in Cha I overlap in position, proper motion, and parallax in good agreement with the findings reported by Roccatagliata et al. (2018).

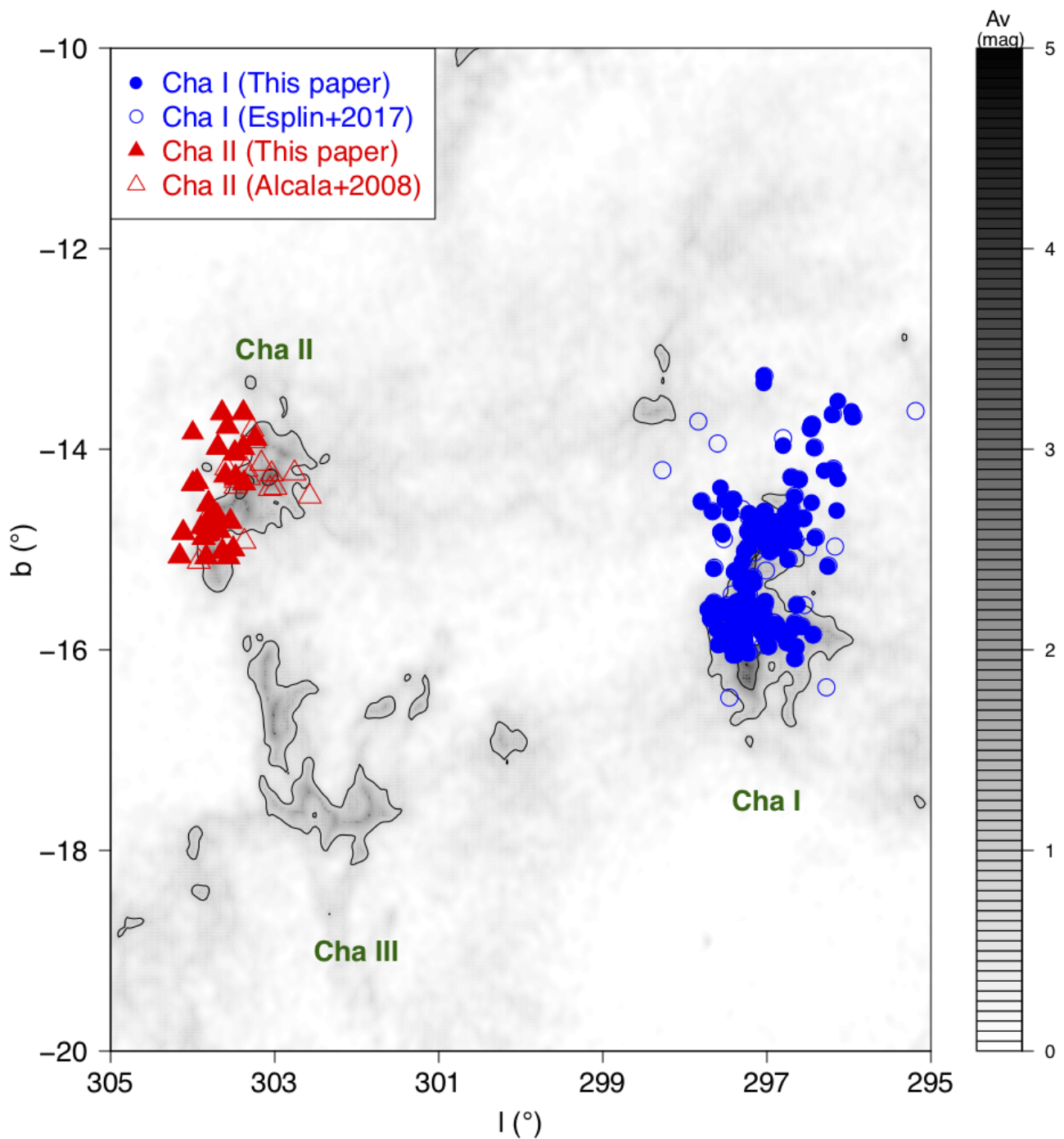


Fig. 3. Location of the Chamaeleon stars overlaid on the extinction map of [Dobashi et al. \(2005\)](#) in Galactic coordinates. Open and filled symbols indicate the position of the stars from the literature ([Alcalá et al. 2008](#); [Esplin et al. 2017](#)) and cluster members identified in this study, respectively. The blue and red colours denote the stars in the Cha I and Cha II molecular clouds, respectively.

In Table 2 we compare the proper motions and parallaxes of the Chamaeleon subgroups in our sample of members. It is apparent from this comparison that the stellar populations in Cha I and Cha II exhibit distinct kinematic properties (as already anticipated in Sect. 2). However, we also note a mean difference of about 1 mas/yr in the proper motions of the stars in the two subgroups of Cha I despite the overlap of the subgroups shown in Figure 9. [Roccatagliata et al. \(2018\)](#) performed a two-sample Kolmogorov-Smirnov test and concluded that the proper motion distribution of the subclusters is not drawn from the same parent

distribution, but the authors do not discuss whether the observed difference is due to projection effects or a different space motion. In Section 3.3 we compute the spatial velocity of the stars and investigate whether the two subclusters in Cha I are indeed kinematically distinct.

3.3. Distance and spatial velocity of Chamaeleon stars

In the following, we convert the stellar proper motions and parallaxes into distances and 2D velocities using Bayesian infer-

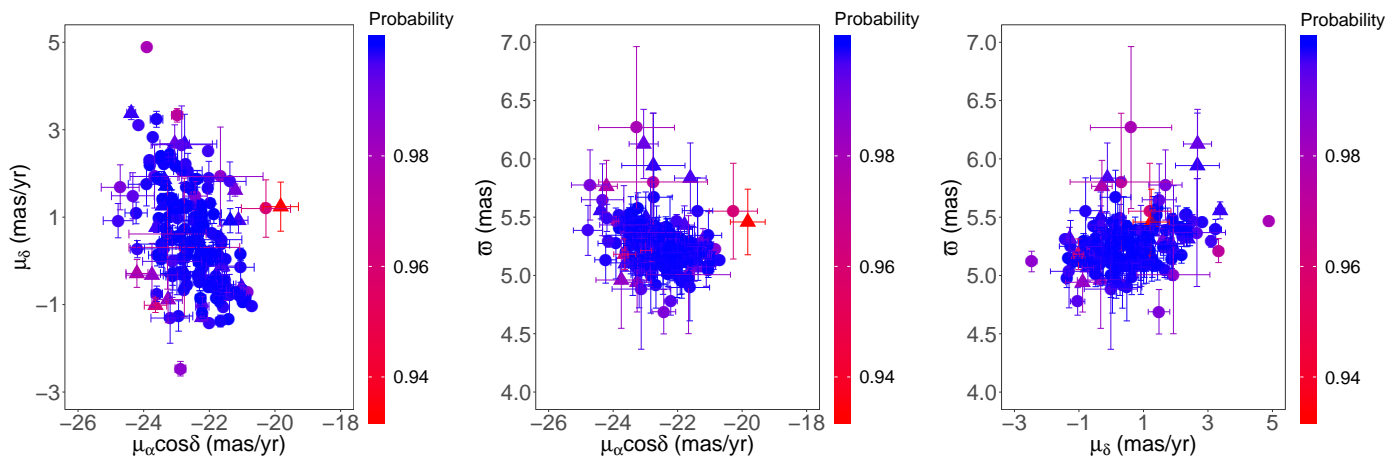


Fig. 4. Proper motions and parallaxes of the 188 stars in Cha I identified in our membership analysis. The stars are colour-coded based on their membership probabilities which are scaled from zero to one. Triangles indicate the stars with $\text{RUWE} \geq 1.4$ (see Sect. 3.1).

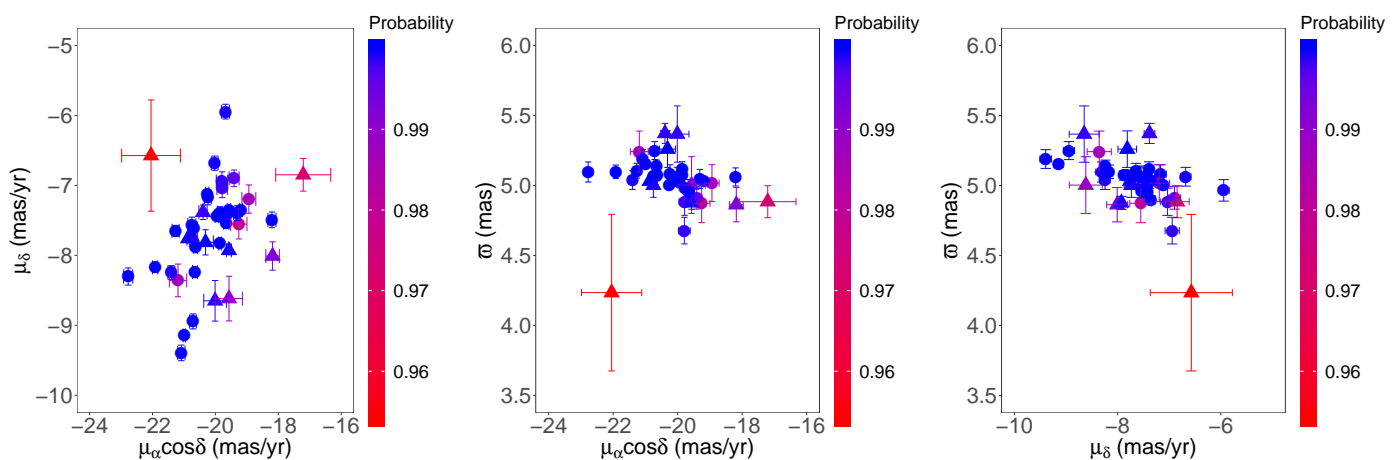


Fig. 5. Proper motions and parallaxes of the 41 stars in Cha II identified in our membership analysis. The stars are colour-coded based on their membership probabilities which are scaled from zero to one. Triangles indicate the stars with $\text{RUWE} \geq 1.4$ (see Sect. 3.1).

Table 2. Proper motions and parallaxes of the Chamaeleon subgroups in our sample of cluster members.

Sample	N_{init}	N_{RUWE}	$\mu_{\alpha} \cos \delta$ (mas/yr)			μ_{δ} (mas/yr)			ϖ (mas)		
			Mean \pm SEM	Median	SD	Mean \pm SEM	Median	SD	Mean \pm SEM	Median	SD
Cha I (north)	87	76	-21.903 ± 0.063	-21.953	0.548	-0.054 ± 0.099	-0.023	0.863	5.178 ± 0.016	5.175	0.138
Cha I (south)	101	84	-23.053 ± 0.069	-23.048	0.629	1.127 ± 0.118	1.022	1.083	5.314 ± 0.023	5.322	0.211
Cha I	188	160	-22.507 ± 0.065	-22.403	0.824	0.566 ± 0.091	0.405	1.146	5.250 ± 0.015	5.235	0.192
Cha II	41	31	-20.207 ± 0.170	-19.954	0.945	-7.635 ± 0.129	-7.491	0.717	5.037 ± 0.021	5.061	0.115

Notes. We provide for each subgroup the initial number of stars, final number of stars after the RUWE filtering (see Sect. 3.1), mean, standard error of the mean (SEM), median and standard deviation (SD) of proper motions and parallaxes.

ence. This analysis uses the *Kalkayotl* package² (Olivares 2019; Olivares et al. 2020) in python programming language, which implements a number of priors for the distance. We took advantage of this code to investigate two priors for the distance that are based on purely statistical probability density distributions (hereafter, statistical priors), and another two priors that are based on astrophysical assumptions (hereafter, astrophysical priors). The statistical priors considered in this paper include the Uniform and Gaussian distributions. The two astrophysical priors that we use are based on the surface brightness profile of

the Large Magellanic Cloud derived from star counts by Elson et al. (1987) and the King’s profile distribution observed in globular clusters (King 1962). More details on the implementation and performance of each prior are given in the *Kalkayotl* paper (Olivares et al. 2020). The prior that we used in the case of the angular velocity (i.e. 2D tangential velocity) is a beta function following the online tutorials available in the *Gaia* archive (Luri et al. 2018). This procedure takes as input the astrometric observables and covariance matrix of the stars as given by the *Gaia*-DR2 catalogue.

We compared the distances derived from different priors and confirmed that they do not depend on the choice of the prior. We

² The code is available at <https://github.com/olivares-j/Kalkayotl>.

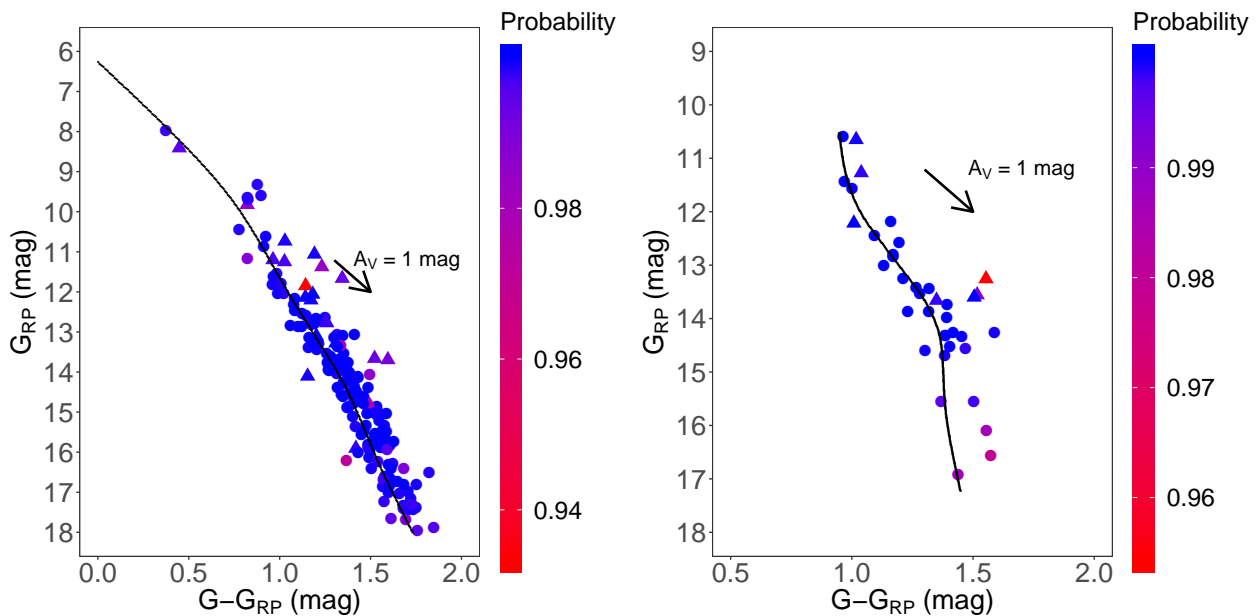


Fig. 6. Colour-magnitude diagram of the cluster members identified in our membership analysis in Cha I (*left panel*) and Cha II (*right panel*). The black solid line indicates the empirical isochrone derived for each cluster (see Tables A.5 and A.6). The stars are colour-coded based on their membership probabilities which are scaled from zero to one. Triangles indicate the stars with $\text{RUWE} \geq 1.4$ (see Sect. 3.1). The arrow indicates the extinction vector of $A_V = 1$ mag that we converted to the Gaia bands based on the relative extinction values computed by Wang & Chen (2019).

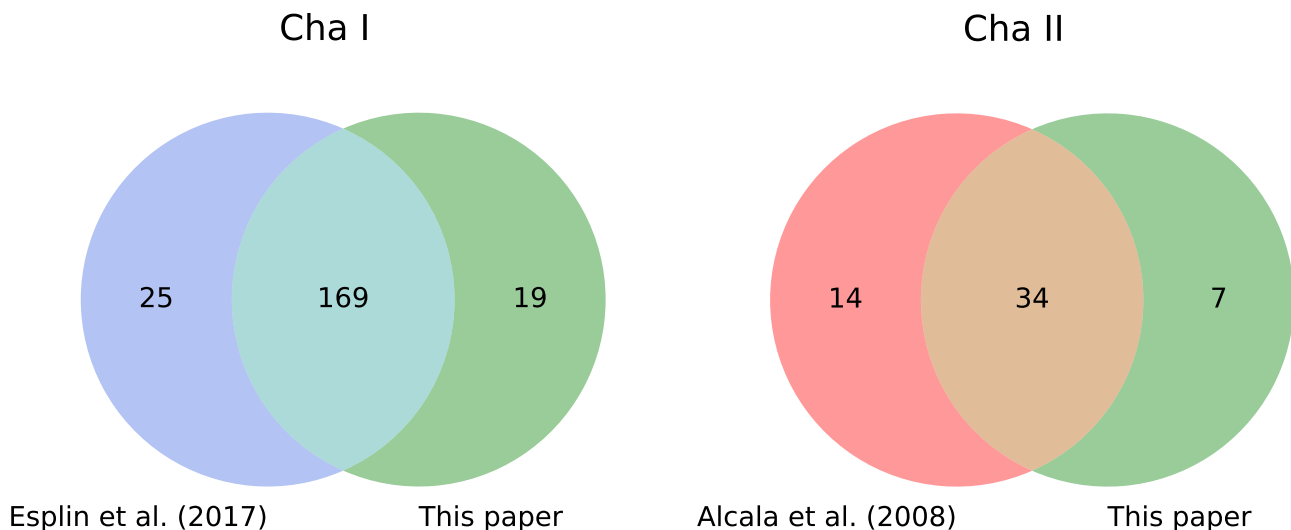


Fig. 7. Venn diagram comparing the number of members (with Gaia-DR2 data) identified in previous studies of the literature (Alcalá et al. 2008; Esplin et al. 2017) and the samples of cluster members derived in this paper from our membership analysis.

therefore decided to report the distances derived from the uniform prior as our final results, because this is the most simple prior. We then used the resulting distances to compute the XYZ position of the stars in a reference system that has its origin at the Sun where X points to the Galactic centre, Y points in the direction of Galactic rotation, and Z points to the Galactic north pole. We converted the 2D tangential velocities and RVs of the stars into the UVW components of the Galactic velocity (in the same reference system described before) using the transformation outlined by Johnson & Soderblom (1987). The distance and spatial velocity of the stars are given in Tables A.1 and A.2.

Table 3 lists the distance of the Chamaeleon subgroups in our sample. We confirm with our methodology that the two subgroups of Cha I (north and south) are located at different distances within the reported uncertainties as previously reported by Roccatagliata et al. (2018). In addition, we measure the distance variation along the line of sight of $\Delta d = 8.1^{+1.3}_{-1.1}$ pc between Cha I and Cha II, and find that they are separated by 23.1 ± 0.3 pc in the space of 3D positions.

The distances derived in this paper based on Gaia-DR2 data are more precise than the results of 179^{+11+11}_{-10-10} pc and 181^{+6+11}_{-5-10} pc obtained by Voirin et al. (2018) for Cha I and Cha II, respectively (the error bars reported in those solutions refer to random

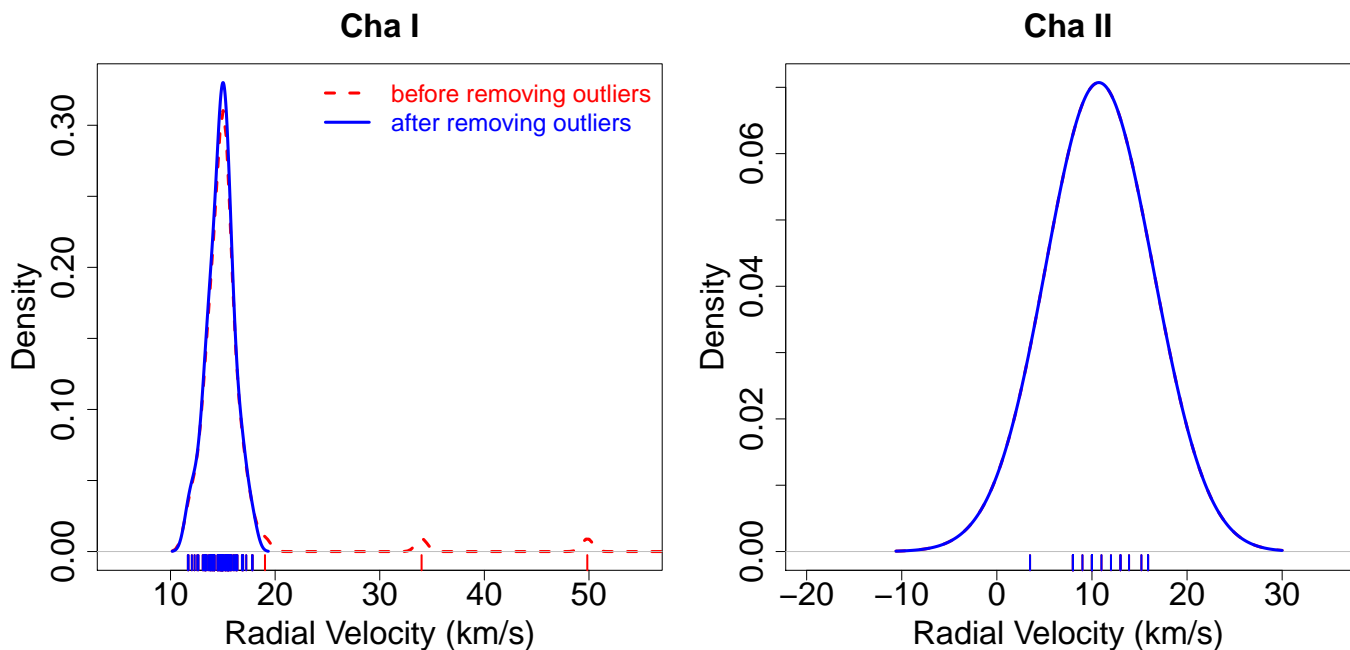


Fig. 8. Kernel density estimate of the RV distribution for the stars in Cha I (left panel) and Cha II (right panel). We used the mean precision of the RVs in each sample (see text in Sect. 3.1) as kernel bandwidth. The tick marks in the horizontal axis mark the RVs of individual stars. The star with the most discrepant RV in the Cha I sample, namely Gaia DR2 5201347408553455616 ($V_r = 164.11 \pm 1.61$ km/s, Sacco et al. 2017), is not shown to improve the visibility of the plot.

Table 3. Distance and spatial velocity of the Chamaeleon subgroups in our sample of cluster members.

Sample	N_d	N_{UVW}	d (pc)	U (km/s)			V (km/s)			W (km/s)		
				Mean	Median	SD	Mean	Median	SD	Mean	Median	SD
Cha I (north)	76	39	$191.4^{+0.8}_{-0.8}$	-10.6 ± 0.4	-10.6	0.7	-19.3 ± 0.6	-19.4	1.0	-11.5 ± 0.2	-11.5	0.6
Cha I (south)	84	39	$186.7^{+1.0}_{-1.0}$	-11.5 ± 0.6	-11.6	0.9	-19.7 ± 0.9	-19.8	1.2	-10.9 ± 0.3	-10.8	0.8
Cha I (all stars)	160	78	$189.4^{+0.8}_{-1.0}$	-11.0 ± 0.5	-11.0	0.9	-19.5 ± 0.8	-19.6	1.1	-11.2 ± 0.3	-11.1	0.8
Cha II (all stars)	31	19	$197.5^{+1.0}_{-0.9}$	-11.0 ± 2.9	-11.2	1.7	-18.1 ± 4.2	-17.8	2.7	-8.5 ± 1.4	-8.6	1.1

Notes. We provide for each subgroup the number of stars used to compute the distance (after the RUWE filtering) and spatial velocity, Bayesian distance, mean, median and standard deviation (SD) of the UVW velocity components. The uncertainties in the mean velocities are computed as explained in the text of Sect. 3.3.

and systematic uncertainties in this order). The latter made use of the parallaxes from the Tycho-Gaia Astrometric Solution catalogue (TGAS, Lindegren et al. 2016) which were affected by systematic errors of about 0.3 mas, which explains the much larger uncertainties in the distances. Our results are more precise than the distances of 192 ± 6 pc and 198 ± 6 provided by Dzib et al. (2018) for Cha I and Cha II, respectively, using different samples of stars. Our distance estimates are also consistent with the results of $192.7^{+0.4}_{-0.4}$ pc and $186.5^{+0.7}_{-0.7}$ pc derived by Roccatagliata et al. (2018) for the northern and southern subclusters of Cha I, respectively. However, in this case we note that our uncertainties are larger by a factor of almost two. As explained in Sect. 2 of Roccatagliata et al. (2018) the authors did not include the systematic errors on the Gaia-DR2 parallaxes in their analysis and derived the distance from the inverse of the parallax. In this study, we derived the distances from Bayesian inference using the *Kalkayotl* code (Olivares et al. 2020) which is designed to deal with some characteristics of the Gaia-DR2 catalogue including the parallax zero-point correction and spatial correlations which are modelled with the covariance function of Vasiliev (2019). The existence of systematic errors in the

Gaia-DR2 catalogue does not compromise the valuable astrometry delivered by the Gaia satellite, but needs to be considered to avoid underestimating uncertainties.

Before computing the distance and spatial velocity of the stars we corrected the Gaia-DR2 parallaxes by the zero-point shift of -0.030 mas and added the systematic errors of 0.1 mas/yr in quadrature to the formal uncertainties on proper motions (see Lindegren et al. 2018, for more details). It is nevertheless important to mention that other zero-point corrections for the Gaia-DR2 parallaxes exist in the literature. They range from -0.031 ± 0.011 mas (Graczyk et al. 2019) to -0.082 ± 0.033 mas (Stassun & Torres 2018). The lowest value is consistent with the zero-point correction provided by the Gaia collaboration (Lindegren et al. 2018), which was adopted throughout this study. We compare in Table 4 the minimum and maximum distances of the Chamaeleon subgroups when we consider different zero-point corrections applied to the Gaia-DR2 parallaxes. The largest zero-point correction available in the literature (-0.082 ± 0.033 mas, Stassun & Torres 2018) puts the Chamaeleon subgroups about 2 pc closer to the Sun, but the resulting distances are still consistent with the results obtained in Table 3 within the reported

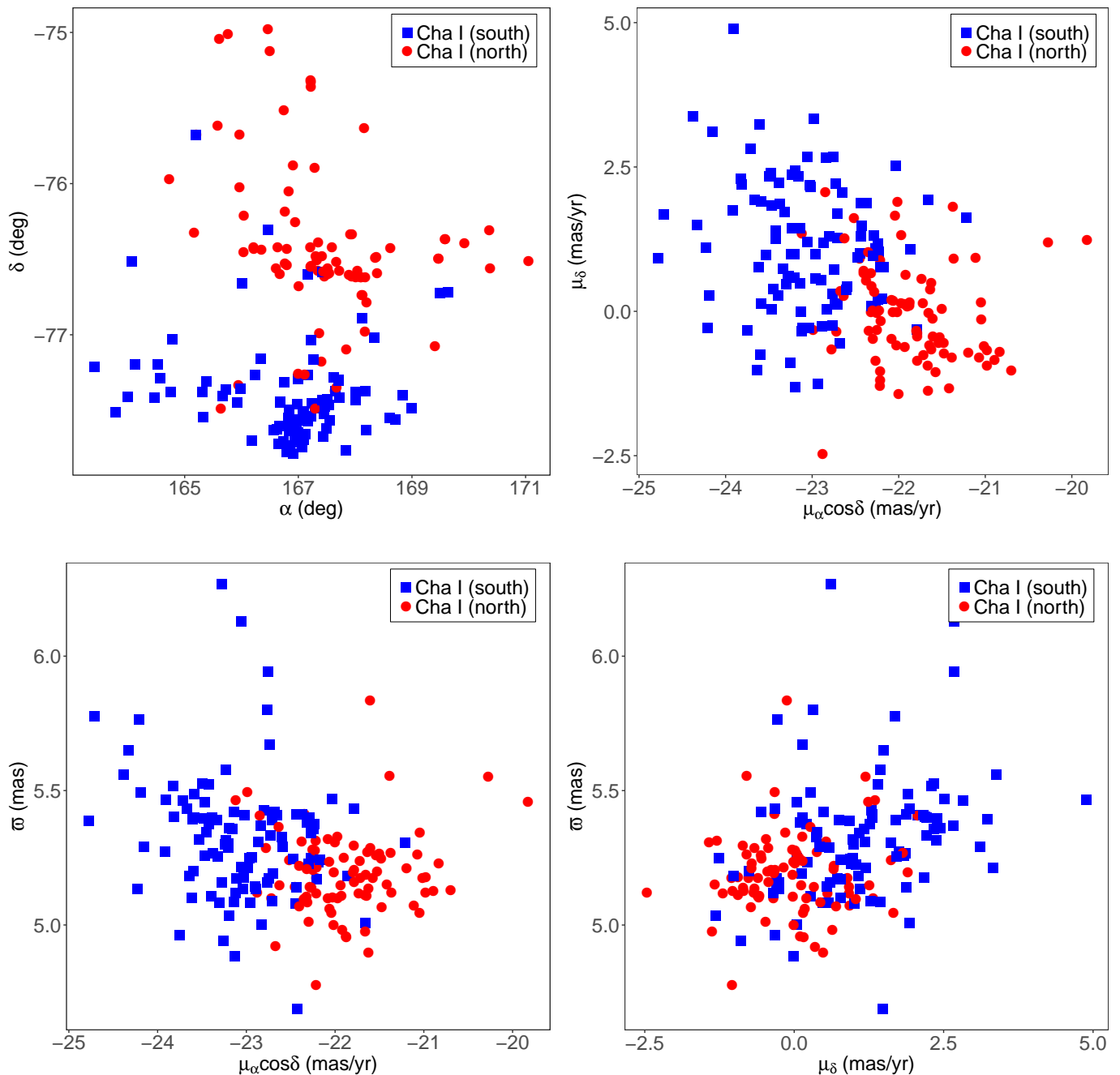


Fig. 9. Clustering results obtained for Cha I with the PAM algorithm in the 5D space of position, proper motion, and parallax.

uncertainties. We therefore conclude that our results are not sensitive to the adopted zero-point correction for the parallaxes.

Although the mean space motion of stellar groups provides useful information, the non-trivial question that arises in our discussion is whether the Chamaeleon subgroups discussed throughout this study are kinematically distinct. In Section 3.2 we report a mean difference of about 1 mas/yr in the proper motions of the two subclusters in Cha I which translates into a relative tangential velocity of the order of 1 km/s. Sacco et al. (2017) also reported a mean difference of about 1 km/s between the RVs of the northern and southern subgroups of Cha I. This relatively small difference in velocity can result from other effects such as for example intrinsic velocity dispersion, undetected bi-

narities, and correlated noise. For example, the transformation of parallaxes, proper motions, and RVs to 3D velocities can result in correlated errors between the velocity components even in the absence of correlations between the astrometric observables (see e.g. Brown et al. 1997; Perryman et al. 1998). We followed the procedure outlined in Sect. 7.2 of Perryman et al. (1998) to investigate this effect in our results. The mean motion of the Chamaeleon subgroups is obtained by averaging the measured velocities and the uncertainty in the mean is computed from the mean of the covariance matrices of the individual stars. The resulting spatial velocities of the Chamaeleon subgroups are given in Table 3. Thus, the relative motion between the two subclusters of Cha I (in the sense ‘north’ minus ‘south’) is $(\Delta U, \Delta V, \Delta W) =$

Table 4. Distance of the Chamaeleon subgroups using different zero-point corrections for the Gaia-DR2 parallaxes.

Sample	N_d	distance (pc)	
		Stassun & Torres (2018)	no correction
Cha I (north)	76	$189.6^{+0.8}_{-0.8}$	$192.5^{+0.8}_{-0.7}$
Cha I (south)	84	$184.9^{+0.9}_{-0.9}$	$187.8^{+0.9}_{-0.9}$
Cha I	160	$187.5^{+0.8}_{-0.8}$	$190.5^{+0.8}_{-0.8}$
Cha II	31	$195.5^{+0.9}_{-0.9}$	$198.6^{+1.0}_{-0.9}$

Notes. We provide for each subgroup the number of stars and the Bayesian distances derived from the largest zero-point shift reported in the literature (-0.082 ± 0.033 mas, Stassun & Torres 2018) and without any zero-point correction applied to the Gaia-DR2 parallaxes.

(0.9, 0.4, -0.6) \pm (0.7, 1.1, 0.4) km/s. Similarly, the relative motion between Cha I and Cha II (in the sense ‘Cha II’ minus ‘Cha I’) is $(\Delta U, \Delta V, \Delta W) = (0.0, 1.4, 2.7) \pm (2.9, 4.3, 1.4)$ km/s. We therefore conclude that the reported differences in the velocity of the subgroups are not significant at the 3σ level when we take into account the covariances in our analysis.

In addition, we also note from Figure 10 that the space motion of most members in the two subclusters of Cha I is consistent within 1σ of the observed velocity dispersion. The observed scatter of the stars in the velocity space results from both measurement errors and the intrinsic velocity dispersion of the cluster. The values listed in Table 3 for the one-dimensional velocity dispersion of Cha I in each velocity component are in good agreement with the velocity dispersion of 1.10 ± 0.15 km/s reported by Sacco et al. (2017) based on the RV of the stars. The median uncertainties in the UVW velocity components of Cha I stars are 0.6, 0.5, and 0.4 km/s, suggesting that the internal velocity dispersion is resolved. On the other hand, the median uncertainties in the three velocity components of Cha II stars are 3.4, 4.7, and 1.8 km/s, implying that the internal velocity dispersion is not resolved. Thus, the observed scatter of Cha II stars in the space of velocities is most probably due to measurement errors and can be explained by the large uncertainties in the RV of the stars (see Sect. 3.1) which propagate to the 3D spatial velocities.

We now compare the space motion of the stellar populations associated with the molecular clouds with the other two young stellar groups located in the Chamaeleon star-forming region. The ϵ Cha and η Cha associations are located in the same sky region of the molecular clouds, but they constitute a foreground population of young stars at a distance of about 100 pc (Gagné et al. 2018b). We cross-matched our samples of Cha I and Cha II stars identified in this study with the lists of ϵ Cha and η Cha given in the literature (see e.g. Gagné et al. 2018a; Gagné & Faherty 2018), but we found no sources in common. The relative motion of Cha I with respect to the space motion of ϵ Cha and η Cha derived by Murphy et al. (2013) is $(\Delta U, \Delta V, \Delta W) = (-0.1, 0.9, -1.3) \pm (0.9, 1.5, 1.4)$ km/s and $(\Delta U, \Delta V, \Delta W) = (-0.8, 1.2, 0.0) \pm (0.5, 0.8, 0.3)$ km/s, respectively (in the sense ‘Cha I’ minus ‘ ϵ Cha’ or ‘ η Cha’). Similarly, the relative motion of Cha II with respect to ϵ Cha and η Cha is $(\Delta U, \Delta V, \Delta W) = (-0.1, 2.3, 1.4) \pm (3.0, 4.4, 2.0)$ km/s and $(\Delta U, \Delta V, \Delta W) = (-0.8, 2.6, 2.7) \pm (2.9, 4.2, 1.4)$ km/s, respectively. Therefore, we conclude that the space motion of ϵ Cha and η Cha is consistent with the space motion of the stars in the Cha I and Cha II molecular clouds within 3σ of the reported uncertainties in the spatial velocities. The common space motion and similar age of the stars in these stellar groups (see e.g. Luhman 2007; Gagné et al. 2018b) suggest that they may have formed

from the same parent cloud, but further investigation study is warranted to confirm this hypothesis.

3.4. Hertzsprung-Russell diagram and relative ages of the subgroups

In this section we use the distances derived from Gaia-DR2 parallaxes (see Sect. 3.3) and spectroscopic data collected from previous studies to construct the most accurate Hertzsprung-Russell diagram (HRD) of the Chamaeleon star-forming region.

We proceed as follows to place the stars in the HRD. First, we compile the spectral types and extinctions for individual stars determined from past studies thanks to the numerous spectroscopic surveys performed in this region. We found spectral types and extinctions for 144 stars (out of 160 stars) in Cha I and 28 stars (out of 31 stars) in Cha II which are given by Esplin et al. (2017) and Spezzi et al. (2008), respectively. Second, we compute the photospheric luminosities from the J -band given by the 2MASS catalogue (Cutri et al. 2003) which is available for all sources with measured spectral type in our sample. We corrected the apparent magnitudes for the extinction values given by Esplin et al. (2017) and Spezzi et al. (2008) using the the extinction relations for various bands given by Cieza et al. (2005) to convert them to the adopted band when necessary. We used the bolometric corrections and effective temperatures for the adopted spectral types given in Table 6 of Pecaut & Mamajek (2013) which is specific for pre-main sequence stars. For a few sources in our sample with spectral types earlier than F0 and later than M5 which are not included in this table we adopt the bolometric corrections and effective temperatures for dwarf stars given in Table 5 of that same study as an approximation. We assumed an uncertainty of half a subclass in the spectral types compiled from the literature which results in an uncertainty of about 20 to 120 K on the effective temperatures for most stars. The resulting stellar luminosities are presented in Table A.7.

Figure 11 shows the HRD with the pre-main sequence star models of Baraffe et al. (2015) and Siess et al. (2000). The two grids of models combined together cover the entire mass domain of our sample which ranges from about 0.02 to 3 M_{\odot} . HD 97048 (Gaia DR2 5201128124701636864) in Cha I is the most massive cluster member in our sample and a A0V Herbig Ae/Be star (see e.g. Chen et al. 2016). Although age determination at these early stages of stellar evolution is rather uncertain, the HRD analysis suggests that the stars in our sample are mostly younger than 5 Myr. In particular, we note that most sources in the HRD are distributed along the 1 Myr isochrone. Some of them are probably binaries or high-order multiple systems that will require further investigation in future studies. However, it is interesting to note that the Chamaeleon stars appear to be younger as compared to previous studies in light of our new analysis based on the stellar distances derived from the Gaia-DR2 parallaxes. For example, the bolometric luminosities derived in this paper are systematically higher than the values obtained by Luhman (2007) who derived the ages of 3-4 Myr and 5-6 Myr for the northern and southern subclusters of Cha I, respectively. The latter study adopted a distance modulus of 6.05 which defines a (common) distance of 162 pc for all stars in the region (i.e., about 30 pc closer to the Sun than the value reported in Table 3) and leads to overestimated ages in the HRD. A similar argument also applies to the results obtained by Spezzi et al. (2008) in Cha II who adopted the distance of 178 ± 18 pc derived by Whittet et al. (1997) to this cloud and reported ages of 3-4 Myr for most sources in their sample. We computed the isochronal age of the stars in our sample by interpolating between the isochrones

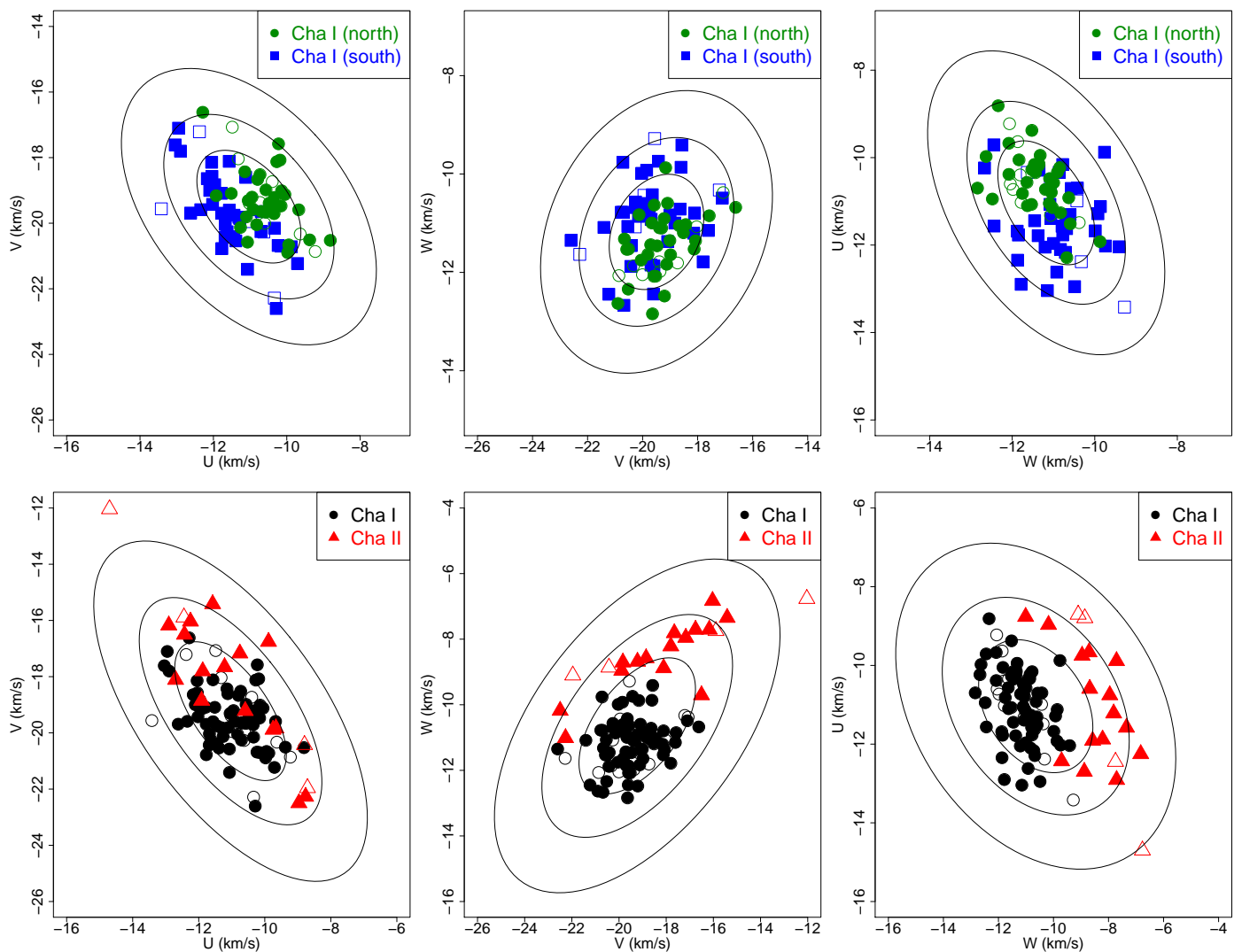


Fig. 10. Distribution of the 3D spatial velocity of Chamaeleon stars. The upper panels compare the velocity of Cha I (north) and Cha I (south), and the lower panels compare the velocity distribution of Cha I and Cha II. Filled and open symbols denote single stars and known binaries (or multiple systems), respectively. The contours indicate the 68.3%, 95.4%, and 99.9% confidence levels computed from the covariance matrix of the ensemble of data points illustrated in each panel.

of the Baraffe et al. (2015) and Siess et al. (2000) models (see Table A.7). This analysis is restricted to the stars covered by these grids of models (see Figure 11). The median age of the Cha I and Cha II subgroups is 1-2 Myr (see Table 5 and discussion below) which suggests that they are indeed younger than previously thought.

Let us now compare the relative ages of the Chamaeleon subgroups based on the fraction of disc-bearing stars in each sample. Luhman et al. (2008) classified the spectral energy distribution (SED) of 122 stars in our sample of 160 cluster members in Cha I based on the spectral index α (Lada 1987) computed from infrared photometry. We compared these results with the ones derived from the classification scheme developed by Koenig & Leisawitz (2014) based on infrared colours from the AllWISE catalogue (Wright et al. 2010). The latter method was originally designed to identify Class I and Class II sources which exhibit strong infrared excess emission as illustrated in Figure 12. We note that many sources in our sample fall into the region between $W2 - W3 < 1.0$ and $W1 - W2 < 0.5$ where Class III and asymptotic giant branch (AGB) stars reside (see e.g. Koenig

& Leisawitz 2014). However, given the very young ages of the stars in our sample (as derived from the HRD) it seems unlikely that these sources are AGB stars and we therefore classify them as Class III stars. When we compare the SED classification derived by Luhman et al. (2008) with the methodology proposed by Koenig & Leisawitz (2014) we find a perfect match for all sources in common between the two methods. By combining the two methodologies we were able to classify the SED of 142 stars in Cha I. We proceeded in a similar manner for the Cha II sample. We compiled the SED classification for 28 stars from the study of Alcalá et al. (2008), and derived the SED subclass for one additional star based on the method of Koenig & Leisawitz (2014).

In Table 5 we compare the fractions of SED classes and age estimates in the Chamaeleon subgroups. This comparison confirms that the two subclusters in Cha I exhibit approximately the same number of Class II and Class III stars as shown previously by Luhman et al. (2008). However, our analysis suggests that the fraction of disc-bearing stars in these subgroups is somewhat lower than the results reported in that study which is also related

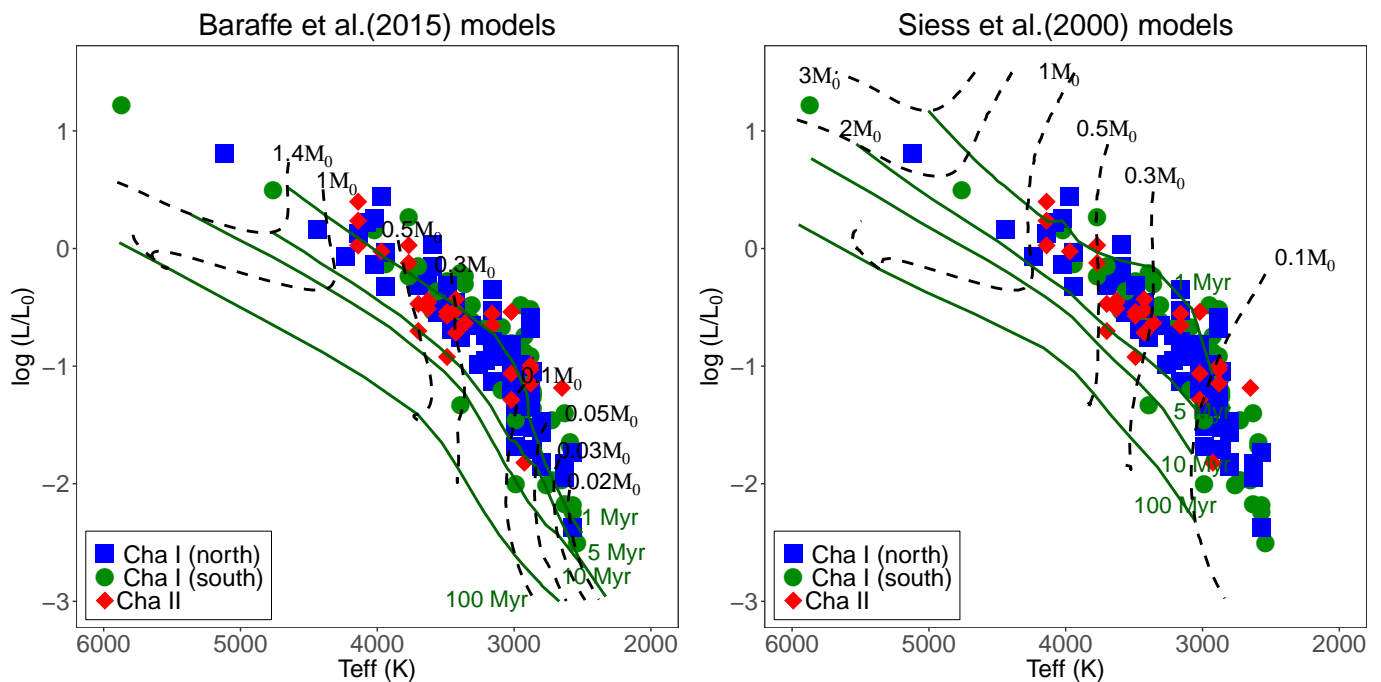


Fig. 11. HRD of the Chamaeleon star-forming region compared to the grid of isochrones and tracks from pre-main sequence stars models. The green solid and black dashed lines denote the isochrones and tracks for each model, respectively, with the ages (in Myr) and masses (in M_{\odot}) indicated in the panels. The different colours and symbols represent the Chamaeleon subgroups discussed throughout this paper. The most massive star in our sample, namely Gaia DR2 5201128124701636864, is not shown here to improve the visibility of the low-mass stars that largely dominate our sample.

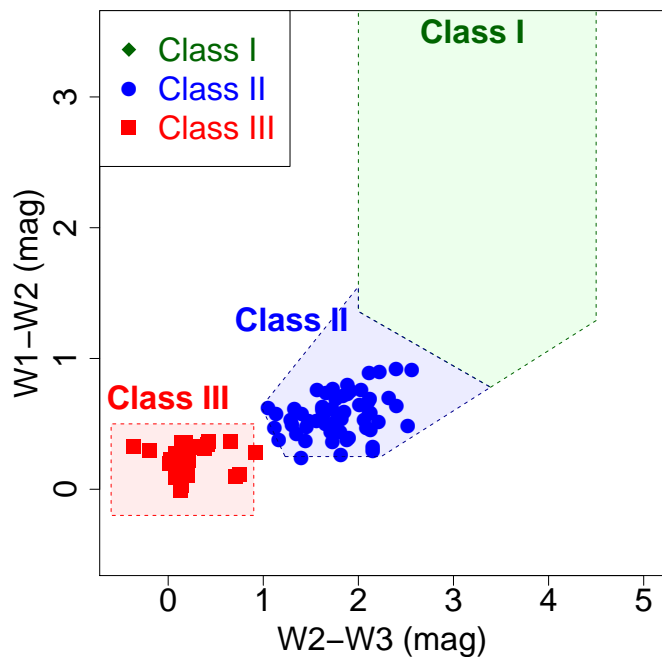


Fig. 12. Colour-colour diagram constructed from infrared colours for the Chamaeleon stars identified in our membership analysis. This is one of the diagrams used in the classification scheme proposed by Koenig & Leisawitz (2014).

to the different samples of stars used in each study. On the other hand, when we compare Cha I and Cha II we see a different

Table 5. Fraction of disc-bearing stars and age estimates of the Chamaeleon subgroups.

Sample	N_{\star}	Class II	Class III	BHAC15 models		SDF00 models	
				N_{\star}	Age (Myr)	N_{\star}	Age (Myr)
Cha I (north)	70	33 (47%)	37 (53%)	33	1.9	49	2.4
Cha I (south)	72	30 (42%)	42 (58%)	30	1.4	53	2.4
Cha I	142	63 (44%)	79 (56%)	63	1.7	102	2.4
Cha II	29	22 (76%)	7 (24%)	15	1.7	23	2.3

Notes. We provide the number of stars and relative fraction of the SED subclasses (in parenthesis), number of stars and median age inferred from Baraffe et al. (2015, BHAC15) and Siess et al. (2000, SDF00) models.

situation. The fraction of disc-bearing stars in Cha II is almost twice as large as in Cha I, although the two populations appear to have similar ages as inferred from the HRD. This suggests that the survival time of circumstellar discs in the Cha I subgroup is somewhat shorter. Similarly, we do not detect significant age differences between the northern and southern subclusters of Cha I. The two SED classes overlap in the 3D space of stellar positions, but the most dispersed cluster members are mostly Class III stars as shown in Figure 13. We find that the two subgroups of Cha I define two parallel filamentary structures with lengths of about 10 pc in the Y direction (see middle panel of Figure 13). We investigated the 3D position of Chamaeleon stars using the distances derived from the different priors discussed in Sect. 3.3 and confirmed that the existence of this structure is not an artifact caused by our choice of prior. The median uncertainties in the XYZ positions of Cha I stars are 1.1, 2.1 and 0.6 pc. The larger uncertainties in Y can be explained by the higher correlation of

the distance with Y ($\rho_Y = -0.95$) as compared to the X and Z coordinates ($\rho_X = 0.73$ and $\rho_Z = -0.09$). Thus, the filamentary structure observed for Cha I is more likely to be explained by the large uncertainties in Y.

We now compare the results obtained in this paper with the ones derived by our team for the Corona-Australis (Galli et al. 2020a) and Lupus (Galli et al. 2020b) star-forming regions using the same methodology applied in this paper. The two age indicators used in this study (isochronal ages and fraction of disc-bearing stars) suggest that the Chamaeleon stars are younger than the stellar population in the Corona-Australis star-forming region. On the other hand, the Chamaeleon subgroups appear to be coeval with the Lupus association and we do not detect important age differences among the various subgroups in these two star-forming regions.

4. Conclusions

In this paper we revise the census of stars with available astrometry in the Gaia-DR2 catalogue that are associated to the molecular clouds of the Chamaeleon star-forming region. We applied a probabilistic method to infer membership probabilities and our analysis allowed us to identify 188 members and 41 members in Cha I and Cha II, respectively. We confirm most of the historical members from the literature (with available Gaia-DR2 astrometry) and increase the samples of cluster members by 11% and 21% in Cha I and Cha II, respectively.

We combined the Gaia-DR2 astrometry with ancillary RV data from previous studies to investigate the 3D spatial distribution and 3D space motion of Chamaeleon stars. We confirm that Cha I and Cha II are located at different distances and are separated by about 23 pc in the 3D space of positions. The two subclusters of Cha I (north and south) are also located at different distances and the observed difference in their proper motion distributions is more likely to be due to projection effects. Our analysis shows that Cha I (north) and Cha I (south) have consistent space motions within the reported uncertainties. The HRD analysis reveals that the stars in our sample are mostly younger than 5 Myr and cover the mass range from 0.02 to 3 M_{\odot} . The median age of the stars is about 1-2 Myr. We detect no significant age differences between Cha I and Cha II, but show that these stellar populations exhibit different fractions of disc-bearing stars. When we compare the results obtained in the present study with those of previous studies conducted by our team in other star-forming regions, we conclude that the Chamaeleon subgroups appear to be coeval with the Lupus association and are younger than the stellar population in the Corona-Australis star-forming region.

In this study we restricted our analysis of the stellar population of the Chamaeleon clouds to the sources with available data in the Gaia-DR2 catalogue. Our team is measuring precise proper motions of faint sources (beyond the sensitivity limit of the *Gaia* satellite) as part of the DANCe project and we will soon be able to expand the current census of Chamaeleon stars based on ancillary data and spectroscopic observations to accurately derive the initial mass function of this stellar group.

Acknowledgements. We thank the referee for constructive criticism that improved the manuscript. This research has received funding from the European Research Council (ERC) under the European Union's Horizon 2020 research and innovation programme (grant agreement No 682903, P.I. H. Bouy), and from the French State in the framework of the "Investments for the future" Program, IdEx Bordeaux, reference ANR-10-IDEX-03-02. This research has made use of the SIMBAD database, operated at CDS, Strasbourg, France. This work has made use of data from the European Space Agency (ESA) mission *Gaia*

(<https://www.cosmos.esa.int/gaia>), processed by the *Gaia* Data Processing and Analysis Consortium (DPAC, <https://www.cosmos.esa.int/web/gaia/dpac/consortium>). Funding for the DPAC has been provided by national institutions, in particular the institutions participating in the *Gaia* Multilateral Agreement. This publication makes use of data products from the Wide-field Infrared Survey Explorer, which is a joint project of the University of California, Los Angeles, and the Jet Propulsion Laboratory/California Institute of Technology, funded by the National Aeronautics and Space Administration.

References

- Alcalá, J. M., Covino, E., Sterzik, M. F., et al. 2000, *A&A*, 355, 629
 Alcalá, J. M., Krautter, J., Schmitt, J. H. M. M., et al. 1995, *A&AS*, 114, 109
 Alcalá, J. M., Spezzi, L., Chapman, N., et al. 2008, *ApJ*, 676, 427
 Allers, K. N., Jaffe, D. T., Luhman, K. L., et al. 2007, *ApJ*, 657, 511
 Baraffe, I., Homeier, D., Allard, F., & Chabrier, G. 2015, *A&A*, 577, A42
 Barrado y Navascués, D. & Jayawardhana, R. 2004, *ApJ*, 615, 840
 Bertout, C., Robichon, N., & Arenou, F. 1999, *A&A*, 352, 574
 Biazzo, K., Alcalá, J. M., Covino, E., et al. 2012, *A&A*, 547, A104
 Bouy, H., Bertin, E., Moraux, E., et al. 2013, *A&A*, 554, A101
 Brown, A. G. A., Perryman, M. A. C., Kovalevsky, J., et al. 1997, in *ESA Special Publication, Vol. 402, Hipparcos - Venice '97*, ed. R. M. Bonnet, E. Høg, P. L. Bernacca, L. Emiliani, A. Blaauw, C. Turon, J. Kovalevsky, L. Lindgren, H. Hassan, M. Bouffard, B. Strim, D. Heger, M. A. C. Perryman, & L. Woltjer, 681–686
 Cambresy, L. 1999, *A&A*, 345, 965
 Cambresy, L., Copet, E., Epchtein, N., et al. 1998, *A&A*, 338, 977
 Cambresy, L., Epchtein, N., Copet, E., et al. 1997, *A&A*, 324, L5
 Carpenter, J. M., Hillenbrand, L. A., Skrutskie, M. F., & Meyer, M. R. 2002, *AJ*, 124, 1001
 Chen, P. S., Shan, H. G., & Zhang, P. 2016, *New A*, 44, 1
 Cieza, L. A., Kessler-Silacci, J. E., Jaffe, D. T., Harvey, P. M., & Evans, Neal J., I. 2005, *ApJ*, 635, 422
 Comerón, F. & Claes, P. 2004, *ApJ*, 602, 298
 Comerón, F., Neuhäuser, R., & Kaas, A. A. 2000, *A&A*, 359, 269
 Comerón, F., Rieke, G. H., & Neuhäuser, R. 1999, *A&A*, 343, 477
 Covino, E., Alcalá, J. M., Allain, S., et al. 1997, *A&A*, 328, 187
 Cutri, R. M., Skrutskie, M. F., van Dyk, S., et al. 2003, *VizieR Online Data Catalog*, II/246
 Dobashi, K., Uehara, H., Kandori, R., et al. 2005, *PASJ*, 57, S1
 Dubath, P., Reipurth, B., & Mayor, M. 1996, *A&A*, 308, 107
 Dziub, S. A., Loïnard, L., Ortiz-León, G. N., Rodríguez, L. F., & Galli, P. A. B. 2018, *ApJ*, 867, 151
 Elson, R. A. W., Fall, S. M., & Freeman, K. C. 1987, *ApJ*, 323, 54
 ESA, . 1997, *VizieR Online Data Catalog*, I/239
 Eplin, T. L., Luhman, K. L., Faherty, J. K., Mamajek, E. E., & Bochanski, J. J. 2017, *AJ*, 154, 46
 Feigelson, E. D., Casanova, S., Montmerle, T., & Guibert, J. 1993, *ApJ*, 416, 623
 Feigelson, E. D. & Lawson, W. A. 2004, *ApJ*, 614, 267
 Fitzgerald, M. P., Stephens, T. C., & Witt, A. N. 1976, *ApJ*, 208, 709
 Franco, G. A. P. 1991, *A&A*, 251, 581
 Gagné, J. & Faherty, J. K. 2018, *ApJ*, 862, 138
 Gagné, J., Mamajek, E. E., Malo, L., et al. 2018a, *ApJ*, 856, 23
 Gagné, J., Roy-Loubier, O., Faherty, J. K., Doyon, R., & Malo, L. 2018b, *ApJ*, 860, 43
 Gaia Collaboration, Brown, A. G. A., Vallenari, A., et al. 2018, *A&A*, 616, A1
 Gaia Collaboration, Brown, A. G. A., Vallenari, A., et al. 2016, *A&A*, 595, A2
 Galli, P. A. B., Bouy, H., Olivares, J., et al. 2020a, *A&A*, 634, A98
 Galli, P. A. B., Bouy, H., Olivares, J., et al. 2020b, *arXiv e-prints*, arXiv:2010.00233
 Gilmore, G., Randich, S., Asplund, M., et al. 2012, *The Messenger*, 147, 25
 Gontcharov, G. A. 2006, *Astronomy Letters*, 32, 759
 Graczyk, D., Pietrzyński, G., Gieren, W., et al. 2019, *ApJ*, 872, 85
 Graham, J. A. & Hartigan, P. 1988, *AJ*, 95, 1197
 Grasdalen, G., Joyce, R., Knacke, R. F., Strom, S. E., & Strom, K. M. 1975, *AJ*, 80, 117
 Gregorio Hetem, J. C., Sanzovo, G. C., & Lepine, J. R. D. 1988, *A&AS*, 76, 347
 Guenther, E. W., Esposito, M., Mundt, R., et al. 2007, *A&A*, 467, 1147
 Hartigan, P. 1993, *AJ*, 105, 1511
 Henize, K. G. & Mendoza, E. E. 1973, *ApJ*, 180, 115
 Hughes, J. & Hartigan, P. 1992, *AJ*, 104, 680
 Hyland, A. R., Jones, T. J., & Mitchell, R. M. 1982, *MNRAS*, 201, 1095
 James, D. J., Melo, C., Santos, N. C., & Bouvier, J. 2006, *A&A*, 446, 971
 Joergens, V. & Guenther, E. 2001, *A&A*, 379, L9
 Johnson, D. R. H. & Soderblom, D. R. 1987, *AJ*, 93, 864
 Kaufmann, L. & Rousseeuw, P. 1987, *Data Analysis based on the L1-Norm and Related Methods*, 405
 King, I. 1962, *AJ*, 67, 471

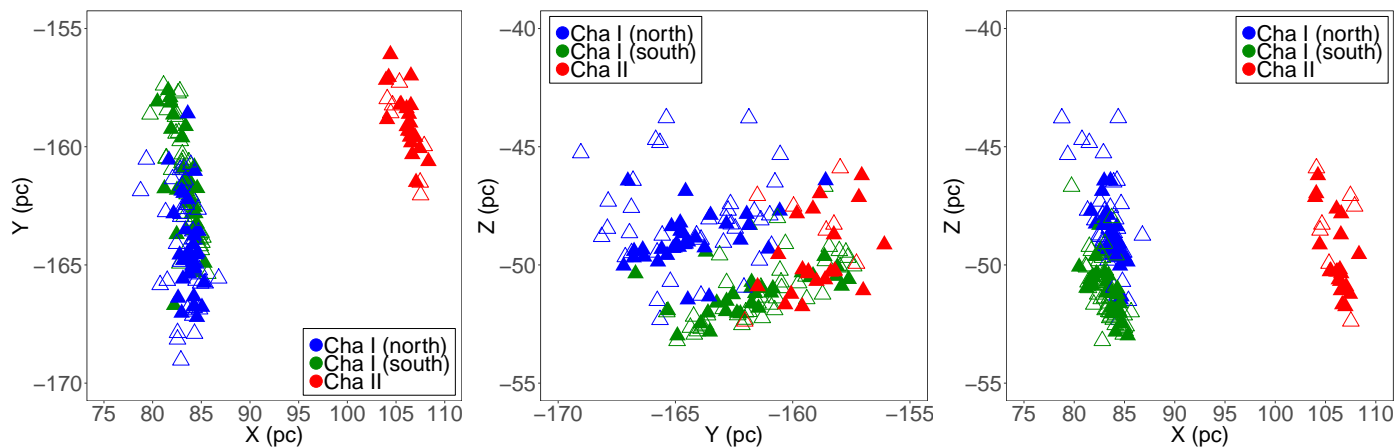


Fig. 13. Spatial distribution of Chamaeleon stars. The different colours denote the subgroups of stars in our sample. Filled and open symbols indicate Class II and Class III stars, respectively.

- Koenig, X. P. & Leisawitz, D. T. 2014, *ApJ*, 791, 131
 Lada, C. J. 1987, in *IAU Symposium*, Vol. 115, *Star Forming Regions*, ed. M. Peimbert & J. Jugaku, 1
 Lindegren, L., Hernández, J., Bombrun, A., et al. 2018, *A&A*, 616, A2
 Lindegren, L., Lammers, U., Bastian, U., et al. 2016, *A&A*, 595, A4
 López Martí, B., Eislöffel, J., & Mundt, R. 2005, *A&A*, 444, 175
 López Martí, B., Eislöffel, J., Scholz, A., & Mundt, R. 2004, *A&A*, 416, 555
 López Martí, B., Jiménez-Esteban, F., Bayo, A., et al. 2013, *A&A*, 556, A144
 López Martí, B., Jiménez Esteban, F., Bayo, A., et al. 2013, *A&A*, 551, A46
 Luhman, K. L. 2004, *ApJ*, 602, 816
 Luhman, K. L. 2007, *ApJS*, 173, 104
 Luhman, K. L. 2008, *Chamaeleon*, ed. B. Reipurth, Vol. 5, 169
 Luhman, K. L., Allen, L. E., Allen, P. R., et al. 2008, *ApJ*, 675, 1375
 Luhman, K. L. & Esplin, T. L. 2020, *AJ*, 160, 44
 Luhman, K. L., Peterson, D. E., & Megeath, S. T. 2004, *ApJ*, 617, 565
 Luri, X., Brown, A. G. A., Sarro, L. M., et al. 2018, *A&A*, 616, A9
 MacQueen, J. 1967, in *Proceedings of the Fifth Berkeley Symposium on Mathematical Statistics and Probability*, Volume 1: *Statistics* (Berkeley, Calif.: University of California Press), 281–297
 Maíz Apellániz, J. & Weiler, M. 2018, *A&A*, 619, A180
 Mizuno, A., Yamaguchi, R., Tachihara, K., et al. 2001, *PASJ*, 53, 1071
 Murphy, S. J., Lawson, W. A., & Bessell, M. S. 2013, *MNRAS*, 435, 1325
 Neuhäuser, R. & Comerón, F. 1998, *Science*, 282, 83
 Neuhäuser, R. & Comerón, F. 1999, *A&A*, 350, 612
 Nguyen, D. C., Brandeker, A., van Kerkwijk, M. H., & Jayawardhana, R. 2012, *ApJ*, 745, 119
 Olivares, J. 2019, *olivares-j/Kalkayotl: Basic functionality*
 Olivares, J., Bouy, H., Sarro, L. M., et al. 2019, *A&A*, 625, A115
 Olivares, J., Sarro, L. M., Bouy, H., et al. 2020, *arXiv e-prints*, arXiv:2010.00272
 Pecaut, M. J. & Mamajek, E. E. 2013, *ApJS*, 208, 9
 Perryman, M. A. C., Brown, A. G. A., Lebreton, Y., et al. 1998, *A&A*, 331, 81
 Persi, P., Marenzi, A. R., Olofsson, G., et al. 2000, *A&A*, 357, 219
 Prusti, T., Whittet, D. C. B., Assendorp, R., & Wesselius, P. R. 1992, *A&A*, 260, 151
 Robrade, J. & Schmitt, J. H. M. M. 2007, *A&A*, 461, 669
 Roccatagliata, V., Sacco, G. G., Franciosini, E., & Randich, S. 2018, *A&A*, 617, L4
 Rousseeuw, P. J. 1987, *Journal of Computational and Applied Mathematics*, 20, 53
 Rousseeuw, P. J. & Driessen, K. V. 1999, *Technometrics*, 41, 212
 Rydgren, A. E. 1980, *AJ*, 85, 444
 Sacco, G. G., Spina, L., Randich, S., et al. 2017, *A&A*, 601, A97
 Sarro, L. M., Bouy, H., Berihuete, A., et al. 2014, *A&A*, 563, A45
 Schwartz, R. D. 1977, *ApJS*, 35, 161
 Schwartz, R. D. 1992, *The Chamaeleon Dark Clouds and T-Associations*, ed. B. Reipurth, 93
 Siess, L., Dufour, E., & Forestini, M. 2000, *A&A*, 358, 593
 Spezzi, L., Alcalá, J. M., Covino, E., et al. 2008, *ApJ*, 680, 1295
 Stassun, K. G. & Torres, G. 2018, *ApJ*, 862, 61
 Stelzer, B., Micela, G., & Neuhäuser, R. 2004, *A&A*, 423, 1029
 Tibshirani, R., Walther, G., & Hastie, T. 2001, *Journal of the Royal Statistical Society: Series B (Statistical Methodology)*, 63, 411
 Torres, C. A. O., Quast, G. R., da Silva, L., et al. 2006, *A&A*, 460, 695
 Vasiliev, E. 2019, *MNRAS*, 489, 623
 Voirin, J., Manara, C. F., & Prusti, T. 2018, *A&A*, 610, A64
 Vuong, M. H., Cambrésy, L., & Epchtein, N. 2001, *A&A*, 379, 208
 Wang, S. & Chen, X. 2019, *ApJ*, 877, 116
 Wenger, M., Ochsenbein, F., Egret, D., et al. 2000, *A&AS*, 143, 9
 Whittet, D. C. B., Prusti, T., Franco, G. A. P., et al. 1997, *A&A*, 327, 1194
 Wright, E. L., Eisenhardt, P. R. M., Mainzer, A. K., et al. 2010, *AJ*, 140, 1868

Appendix A: Tables (online material)

Table A.1. Properties of the 188 cluster members selected from our membership analysis in Cha I. (This table will be available in its entirety in machine-readable form.)

Source Identifier	α (h:m:s)	δ ($^{\circ}$ ' ")	$\mu_{\alpha} \cos \delta$ (mas/yr)	μ_{δ} (mas/yr)	ϖ (mas)	RUWE	Prob.	V_r (km/s)	Ref	d (pc)	U (km/s)	V (km/s)	W (km/s)	Cloud	SED
Gaia DR2 5201384581492347904	10 53 39.65	-77 12 33.9	-22.980 \pm 0.172	3.329 \pm 0.154	5.213 \pm 0.103	1.08	0.9723			190.8 ^{+2.9} _{-3.1}				Cha I (south)	
Gaia DR2 5201001852664912512	10 55 09.54	-77 30 54.2	-22.210 \pm 0.136	0.771 \pm 0.120	5.170 \pm 0.071	1.32	1.0000	16.83 \pm 0.90	1	192.1 ^{+2.5} _{-2.5}	-10.2 ^{+0.9} _{-0.9}	-20.7 ^{+1.0} _{-1.0}	-12.7 ^{+0.6} _{-0.6}	Cha I (south)	Class III
Gaia DR2 5201378641555926656	10 55 59.05	-77 24 39.4	-23.904 \pm 0.077	4.889 \pm 0.072	5.466 \pm 0.041	1.31	0.9794			184.3 ^{+1.3} _{-1.2}				Cha I (south)	
Gaia DR2 5201378641555926784	10 55 59.69	-77 24 40.1	-23.813 \pm 0.059	2.193 \pm 0.053	5.403 \pm 0.031	1.21	0.9998			185.6 ^{+1.6} _{-1.4}				Cha I (south)	
Gaia DR2 5201536661993294720	10 56 16.28	-76 30 53.1	-22.712 \pm 0.180	1.275 \pm 0.160	5.089 \pm 0.106	1.22	0.9999	12.56 \pm 2.01	1	192.6 ^{+2.0} _{-2.0}	-13.0 ^{+1.5} _{-1.5}	-17.6 ^{+2.0} _{-2.0}	-11.1 ^{+1.0} _{-1.0}	Cha I (south)	Class II
Gaia DR2 5201388292344009984	10 56 30.28	-77 11 39.4	-23.714 \pm 0.037	2.822 \pm 0.035	5.462 \pm 0.019	1.07	0.9993	15.30 \pm 0.03	2	184.1 ^{+1.2} _{-1.0}	-11.6 ^{+0.3} _{-0.4}	-20.3 ^{+0.2} _{-0.5}	-10.7 ^{+0.3} _{-0.3}	Cha I (south)	
Gaia DR2 5201191037382571904	10 57 53.66	-77 24 49.7	-23.477 \pm 0.092	2.389 \pm 0.080	5.397 \pm 0.049	1.20	0.9999	15.71 \pm 0.32	1	186.1 ^{+2.1} _{-1.8}	-11.4 ^{+0.6} _{-0.6}	-20.5 ^{+0.5} _{-0.5}	-11.1 ^{+0.4} _{-0.4}	Cha I (south)	
Gaia DR2 5201387776948008320	10 58 05.86	-77 11 50.1	-23.199 \pm 0.231	2.441 \pm 0.204	5.360 \pm 0.104	1.00	0.9999			188.0 ^{+3.3} _{-3.0}				Cha I (south)	Class II
Gaia DR2 5201199348142249216	10 58 16.64	-77 17 17.2	-23.375 \pm 0.081	1.865 \pm 0.070	5.267 \pm 0.042	2.17	0.9993			191.1 ^{+1.9} _{-1.9}				Cha I (south)	
Gaia DR2 5201199352439663872	10 58 17.95	-77 17 19.9	-22.369 \pm 0.166	1.878 \pm 0.192	5.412 \pm 0.091	1.22	0.9999			186.7 ^{+3.1} _{-2.3}				Cha I (south)	
Gaia DR2 5201568891428175872	10 58 54.74	-75 58 19.6	-22.403 \pm 0.111	0.704 \pm 0.083	5.070 \pm 0.058	1.17	0.9999			193.6 ^{+1.4} _{-2.0}				Cha I (north)	Class III
Gaia DR2 5201196599363180928	10 59 00.95	-77 22 40.9	-23.385 \pm 0.036	2.220 \pm 0.033	5.399 \pm 0.019	1.07	0.9998	17.80 \pm 0.10	3	186.2 ^{+1.4} _{-1.4}	-10.3 ^{+0.5} _{-0.5}	-22.3 ^{+0.3} _{-0.3}	-11.6 ^{+0.3} _{-0.3}	Cha I (south)	
Gaia DR2 5201226389256838528	10 59 06.87	-77 01 40.3	-22.726 \pm 0.050	2.217 \pm 0.044	5.334 \pm 0.023	1.10	0.9989	14.99 \pm 0.06	2	187.1 ^{+1.6} _{-1.6}	-11.3 ^{+0.4} _{-0.4}	-19.8 ^{+0.2} _{-0.2}	-10.6 ^{+0.3} _{-0.3}	Cha I (south)	
Gaia DR2 5201553704423697792	11 00 40.14	-76 19 28.0	-22.404 \pm 0.076	0.664 \pm 0.064	5.221 \pm 0.043	1.09	1.0000	15.69 \pm 0.03	2	192.2 ^{+1.8} _{-1.9}	-10.8 ^{+0.4} _{-0.4}	-20.0 ^{+0.2} _{-0.2}	-11.8 ^{+0.3} _{-0.3}	Cha I (north)	Class II
Gaia DR2 5225597893420402176	11 00 46.99	-75 40 36.4	-22.753 \pm 0.981	2.673 \pm 0.680	5.943 \pm 0.450	4.90	0.9985			187.5 ^{+4.7} _{-3.2}				Cha I (south)	
Gaia DR2 5225597889120103424	11 00 49.18	-75 40 41.4	-22.042 \pm 0.139	1.660 \pm 0.098	5.045 \pm 0.063	1.10	0.9994			193.6 ^{+1.4} _{-1.8}				Cha I (north)	
Gaia DR2 5201194816953813504	11 01 13.58	-77 22 38.7	-23.609 \pm 0.193	3.238 \pm 0.182	5.395 \pm 0.086	1.08	0.9993			187.0 ^{+3.0} _{-2.5}				Cha I (south)	Class III
Gaia DR2 5201185574182015744	11 01 19.09	-77 32 38.7	-22.653 \pm 0.435	2.062 \pm 0.397	5.408 \pm 0.188	0.98	0.9992			187.9 ^{+4.1} _{-3.7}				Cha I (south)	Class III
Gaia DR2 5201185574184171776	11 01 19.31	-77 32 37.5	-23.668 \pm 0.748	1.931 \pm 0.723	5.433 \pm 0.337	1.24	0.9951			188.5 ^{+4.4} _{-3.7}				Cha I (south)	
Gaia DR2 5201218864474119808	11 01 31.93	-77 18 25.0	-24.715 \pm 0.578	1.682 \pm 0.515	5.776 \pm 0.301	1.04	0.9903			187.0 ^{+4.4} _{-2.8}				Cha I (south)	Class III

Notes. For each star, we provide the Gaia-DR2 identifier, position, proper motion and parallax (not corrected for zero-point offset) from the Gaia-DR2 catalogue, RUWE value, membership probability, RV with reference, distance derived from Bayesian inference, UVW spatial velocity, molecular cloud, and SED class. References for radial velocities are: (1) [Sacco et al. \(2017\)](#), (2) [Nguyen et al. \(2012\)](#), (3) [Guenther et al. \(2007\)](#), and (4) [Joergens & Guenther \(2001\)](#).

Table A.2. Properties of the 41 cluster members selected from our membership analysis in Cha II. (This table will be available in its entirety in machine-readable form.)

Source Identifier	α (h:m:s)	δ ($^{\circ}$ ' ")	$\mu_{\alpha} \cos \delta$ (mas/yr)	μ_{δ} (mas/yr)	ϖ (mas)	RUWE	Prob.	V_r (km/s)	Ref	d (pc)	U (km/s)	V (km/s)	W (km/s)	Cloud	SED
Gaia DR2 5789146187323908736	12 56 33.55	-76 45 45.6	-21.265 \pm 0.113	-7.648 \pm 0.077	5.106 \pm 0.052	1.14	1.0000	15.90 \pm 0.50	1	195.6 $^{+2.3}_{-2.0}$	-9.0 $^{+0.7}_{-0.7}$	-22.5 $^{+0.7}_{-0.7}$	-10.2 $^{+0.4}_{-0.4}$	Cha II	Class II
Gaia DR2 5789258681110332416	12 58 56.05	-76 30 10.7	-21.082 \pm 0.117	-9.394 \pm 0.112	5.189 \pm 0.067	1.01	0.9999	9.00 \pm 5.40	1	194.7 $^{+2.0}_{-1.9}$	-12.4 $^{+3.4}_{-3.4}$	-16.5 $^{+4.7}_{-4.7}$	-9.7 $^{+0.4}_{-1.6}$	Cha II	Class III
Gaia DR2 5788954902364046848	12 59 09.78	-76 51 03.9	-21.189 \pm 0.276	-8.357 \pm 0.234	5.242 \pm 0.147	1.01	0.9872			195.5 $^{+3.2}_{-2.5}$				Cha II	Class II
Gaia DR2 5788930820483641088	12 59 10.05	-77 12 14.0	-22.775 \pm 0.146	-8.302 \pm 0.122	5.096 \pm 0.072	1.01	0.9999			196.0 $^{+2.8}_{-2.3}$				Cha II	Class III
Gaia DR2 5788932607187147136	13 00 53.14	-77 09 09.4	-20.751 \pm 0.130	-7.734 \pm 0.138	5.002 \pm 0.087	1.62	0.9995			198.6 $^{+2.6}_{-3.0}$				Cha II	
Gaia DR2 5789044482500658560	13 00 53.15	-76 54 15.3	-20.653 \pm 0.076	-8.238 \pm 0.062	5.137 \pm 0.044	1.20	1.0000			194.3 $^{+1.8}_{-1.6}$				Cha II	Class II
Gaia DR2 5788932607187147264	13 00 53.49	-77 09 08.5	-21.401 \pm 0.110	-8.245 \pm 0.099	5.039 \pm 0.067	1.05	0.9997			197.8 $^{+1.6}_{-2.8}$				Cha II	
Gaia DR2 5788932778988729856	13 00 55.24	-77 08 29.8	-21.916 \pm 0.085	-8.171 \pm 0.068	5.098 \pm 0.048	1.00	1.0000	10.00 \pm 6.00	1	195.8 $^{+2.2}_{-2.0}$	-12.7 $^{+3.7}_{-3.7}$	-18.1 $^{+5.2}_{-5.2}$	-8.9 $^{+1.8}_{-1.8}$	Cha II	Class III
Gaia DR2 5789044478200012160	13 00 56.14	-76 54 02.5	-19.570 \pm 0.078	-7.927 \pm 0.063	4.876 \pm 0.046	1.66	0.9998			201.4 $^{+1.6}_{-1.6}$				Cha II	
Gaia DR2 5788090759241383680	13 01 58.80	-77 51 22.0	-20.869 \pm 0.038	-7.759 \pm 0.031	5.030 \pm 0.020	1.44	1.0000			195.9 $^{+1.7}_{-1.7}$				Cha II	
Gaia DR2 5789239989411572608	13 02 13.43	-76 37 58.0	-20.990 \pm 0.040	-9.144 \pm 0.041	5.152 \pm 0.024	1.15	0.9999	15.90 \pm 1.10	2	194.1 $^{+1.5}_{-1.5}$	-8.8 $^{+1.0}_{-1.0}$	-22.3 $^{+1.2}_{-1.2}$	-11.0 $^{+0.5}_{-0.5}$	Cha II	Class II
Gaia DR2 5788861173293937792	13 02 22.75	-77 34 49.6	-19.786 \pm 0.165	-7.035 \pm 0.139	4.884 \pm 0.097	1.01	0.9984	12.00 \pm 7.20	1	200.3 $^{+2.1}_{-2.6}$	-10.6 $^{+4.4}_{-4.6}$	-19.2 $^{+6.2}_{-6.3}$	-8.7 $^{+2.2}_{-2.3}$	Cha II	Class II
Gaia DR2 5789026065680783104	13 03 04.36	-77 07 02.9	-20.011 \pm 0.361	-8.649 \pm 0.290	5.367 \pm 0.201	6.78	0.9991			195.6 $^{+3.3}_{-2.5}$				Cha II	
Gaia DR2 5788087666864871168	13 03 08.96	-77 55 59.7	-19.791 \pm 0.181	-6.943 \pm 0.138	4.677 \pm 0.095	1.22	0.9990	11.00 \pm 6.60	1	201.4 $^{+1.8}_{-2.0}$	-11.9 $^{+4.2}_{-4.3}$	-18.9 $^{+5.7}_{-5.8}$	-8.6 $^{+2.1}_{-2.2}$	Cha II	Class III
Gaia DR2 5789245005933444096	13 03 16.08	-76 29 38.2	-19.677 \pm 0.127	-5.945 \pm 0.105	4.965 \pm 0.077	1.03	0.9997			199.6 $^{+2.3}_{-2.7}$				Cha II	Class III
Gaia DR2 5789045856890263936	13 04 22.76	-76 50 05.6	-19.954 \pm 0.054	-7.434 \pm 0.046	5.025 \pm 0.029	1.02	1.0000			197.1 $^{+1.9}_{-1.8}$				Cha II	Class II
Gaia DR2 5789045856890265216	13 04 24.02	-76 50 01.3	-20.258 \pm 0.050	-7.117 \pm 0.044	5.003 \pm 0.026	1.03	0.9999	15.20 \pm 0.20	1	198.0 $^{+1.8}_{-1.8}$	-8.7 $^{+0.5}_{-0.5}$	-22.0 $^{+0.5}_{-0.4}$	-9.1 $^{+0.3}_{-0.3}$	Cha II	Class II
Gaia DR2 5788088457138909056	13 04 24.77	-77 52 30.4	-19.406 \pm 0.158	-6.898 \pm 0.119	4.911 \pm 0.080	1.21	0.9963	13.00 \pm 7.80	1	199.4 $^{+2.4}_{-2.9}$	-9.7 $^{+4.8}_{-4.7}$	-19.8 $^{+6.7}_{-6.6}$	-8.7 $^{+2.4}_{-2.4}$	Cha II	Class II
Gaia DR2 5788199129851179392	13 04 55.62	-77 39 51.0	-19.568 \pm 0.427	-8.617 \pm 0.319	5.003 \pm 0.203	1.98	0.9889			197.9 $^{+3.9}_{-3.3}$				Cha II	
Gaia DR2 5788199129856209792	13 04 55.62	-77 39 49.3	-20.629 \pm 0.054	-7.880 \pm 0.046	5.071 \pm 0.033	1.13	1.0000			196.7 $^{+1.9}_{-1.9}$				Cha II	Class II

Notes. For each star, we provide the Gaia-DR2 identifier, position, proper motion and parallax (not corrected for zero-point offset) from the Gaia-DR2 catalogue, RUWE value, membership probability, RV with reference, distance derived from Bayesian inference, UVW spatial velocity, molecular cloud, and SED class. References for radial velocities are: (1) [Biazzo et al. \(2012\)](#), (2) [Torres et al. \(2006\)](#), and (3) Gaia-DR2.

Table A.3. Membership probability of all sources in the field derived independently using different p_{in} values in the membership analysis conducted for Cha I. (This table will be available in its entirety in machine-readable form.)

Source Identifier	probability ($p_{in} = 0.5$)	probability ($p_{in} = 0.6$)	probability ($p_{in} = 0.7$)	probability ($p_{in} = 0.8$)	probability ($p_{in} = 0.9$)
Gaia DR2 5201074042471837568	1.4349E-147	2.7899E-149	5.4960E-151	7.4803E-152	5.5727E-157
Gaia DR2 5201073836316342528	8.6941E-281	2.9651E-282	4.4077E-284	5.4432E-292	1.6288E-294
Gaia DR2 5201073836313415424	4.3543E-109	1.1548E-109	3.3785E-112	6.4841E-113	1.9674E-118
Gaia DR2 5201073935099216512	1.0370E-187	4.3339E-190	3.6931E-193	8.3850E-197	9.3870E-203
Gaia DR2 5201073836316344320	2.3984E-298	2.3984E-298	2.3984E-298	2.3983E-298	2.3983E-298
Gaia DR2 5201073935099219072	3.6232E-116	2.6937E-117	5.4370E-119	1.8111E-119	1.0402E-123
Gaia DR2 5201073832019988480	9.1292E-259	9.9697E-261	1.8108E-264	2.4042E-269	2.1896E-278
Gaia DR2 5201073939393526528	1.5073E-17	1.4872E-17	9.2370E-18	6.6952E-18	1.7472E-18
Gaia DR2 5201073935099210240	1.9355E-106	2.9213E-107	6.1859E-109	1.8016E-109	9.9123E-114
Gaia DR2 5201073935099216128	1.4987E-168	2.5022E-169	1.7000E-172	7.1575E-174	1.7152E-181
Gaia DR2 5201073832019985536	5.7921E-186	8.4142E-187	6.1339E-190	3.3510E-192	1.2762E-199
Gaia DR2 5201073973755611904	2.3469E-76	1.3902E-76	1.5145E-78	7.1632E-79	2.7975E-83
Gaia DR2 5201073939393029632	6.6388E-126	6.1494E-126	3.7579E-127	8.4288E-128	4.6618E-131
Gaia DR2 5201074351710395392	1.6818E-83	1.6836E-83	1.0307E-84	3.9460E-85	1.5117E-88
Gaia DR2 5201073935102778624	1.4768E-297	1.4768E-297	1.4768E-297	1.4767E-297	1.4767E-297
Gaia DR2 5201073969459128320	6.1980E-30	6.3911E-30	1.8565E-30	1.3947E-30	5.7569E-32
Gaia DR2 5201074381775839872	3.6815E-297	3.1125E-298	3.1069E-298	3.1069E-298	3.1069E-298
Gaia DR2 5201074347416098560	3.6472E-78	2.2980E-78	1.4179E-79	4.7970E-80	5.5506E-83
Gaia DR2 5201073939393531648	2.3397E-81	1.5185E-81	2.8149E-83	1.4863E-83	6.8345E-88
Gaia DR2 5201073973752401664	1.7528E-212	6.1688E-215	1.3509E-217	6.8561E-220	7.4386E-228

Table A.4. Membership probability of all sources in the field derived independently using different p_{in} values in the membership analysis conducted for Cha II. (This table will be available in its entirety in machine-readable form.)

Source Identifier	probability ($p_{in} = 0.5$)	probability ($p_{in} = 0.6$)	probability ($p_{in} = 0.7$)	probability ($p_{in} = 0.8$)	probability ($p_{in} = 0.9$)
Gaia DR2 5789212089299174016	5.0757E-58	2.3736E-59	2.3849E-59	9.2531E-58	2.3516E-59
Gaia DR2 5789212089301993216	3.7768E-293	3.7767E-293	3.7767E-293	3.7767E-293	3.7767E-293
Gaia DR2 5789211161587017600	1.3585E-23	9.7102E-24	9.7266E-24	2.9880E-24	9.6661E-24
Gaia DR2 5789211157294203008	1.7804E-10	1.6458E-10	1.6459E-10	1.6232E-10	1.6454E-10
Gaia DR2 5789210951131853824	1.5332E-98	8.5218E-100	8.6591E-100	7.8309E-89	8.2448E-100
Gaia DR2 5789163882589260416	6.2073E-21	7.1975E-21	7.2019E-21	1.1882E-20	7.1882E-21
Gaia DR2 5789211157294205056	3.9985E-152	3.8209E-153	4.0248E-153	2.7734E-139	3.4379E-153
Gaia DR2 5789163500333081344	1.7415E-61	6.7563E-61	6.8618E-61	9.2221E-58	6.5271E-61
Gaia DR2 5789211157290990080	2.7402E-79	1.3261E-79	1.3710E-79	4.7306E-84	1.2402E-79
Gaia DR2 5789212085003280512	5.2980E-204	1.1604E-204	1.3612E-204	5.1170E-224	8.4274E-205
Gaia DR2 5789210951131856128	2.7245E-224	2.1403E-224	2.3742E-224	1.1483E-201	1.7413E-224
Gaia DR2 5789163672132325504	1.9522E-32	1.6995E-32	1.7025E-32	1.1393E-31	1.6931E-32
Gaia DR2 5789210951131851008	6.0084E-60	6.2951E-61	6.3458E-61	3.4878E-62	6.1709E-61
Gaia DR2 5789163672131796864	9.6607E-121	2.4770E-121	2.6914E-121	1.3474E-112	2.0736E-121
Gaia DR2 5789163500333632256	6.0395E-62	1.5696E-61	1.5891E-61	1.8863E-57	1.5279E-61
Gaia DR2 5789163878290242176	8.1662E-297	8.1659E-297	8.1659E-297	8.1659E-297	8.1659E-297
Gaia DR2 5789162400824292224	1.0405E-06	2.5707E-07	2.5707E-07	2.6156E-07	2.5709E-07
Gaia DR2 5789212020582705536	2.7468E-34	1.7392E-34	1.7444E-34	3.6916E-35	1.7262E-34
Gaia DR2 5789211195946756736	7.1236E-20	5.6508E-20	5.6523E-20	5.8063E-20	5.6475E-20
Gaia DR2 5789210951131859072	1.7569E-108	7.4057E-110	7.7175E-110	4.9623E-108	6.8126E-110

Table A.5. Empirical isochrone of Cha I inferred from our membership analysis. (This table will be available in its entirety in machine-readable form.)

G_{RP} (mag)	$G - G_{RP}$ (mag)
6.143	-0.027
6.175	-0.020
6.207	-0.012
6.239	-0.005
6.271	0.003
6.303	0.010
6.335	0.018
6.366	0.025
6.398	0.033
6.430	0.040
6.462	0.048
6.494	0.055
6.526	0.063
6.558	0.070
6.590	0.078
6.622	0.085
6.654	0.093
6.686	0.100
6.718	0.107
6.750	0.115

Table A.6. Empirical isochrone of Cha II inferred from our membership analysis. (This table will be available in its entirety in machine-readable form.)

G_{RP} (mag)	$G - G_{RP}$ (mag)
10.528	0.949
10.544	0.949
10.561	0.950
10.578	0.950
10.595	0.951
10.612	0.951
10.629	0.952
10.646	0.952
10.663	0.953
10.679	0.953
10.696	0.954
10.713	0.954
10.730	0.954
10.747	0.955
10.764	0.955
10.781	0.956
10.798	0.956
10.814	0.957
10.831	0.957
10.848	0.958

Table A.7. Stellar parameters for the HRD analysis. (This table will be available in its entirety in machine-readable form.)

Gaia-DR2 Identifier	α (h:m:s)	δ ($^{\circ}$ ' ")	J	A_J (mag)	SpT (mag)	T_{eff} (K)	L_{\star} (L_{\odot})	t_{BHAC15} (Myr)	t_{SDF00} (Myr)	Subgroup
Gaia DR2 5201384581492347904	10 53 39.65	-77 12 33.9	13.282 \pm 0.024	0.63	M2.75	3392 \pm 82	0.047 ^{+0.002} _{-0.003}	15.8 ^{+8.6} _{-6.5}	13.6 ^{+3.4} _{-4.0}	Cha I (south)
Gaia DR2 5201001852664912512	10 55 09.54	-77 30 54.2	11.881 \pm 0.024	0.34	M4.5	3020 \pm 120	0.117 ^{+0.006} _{-0.010}		2.7 ^{+0.0} _{-0.0}	Cha I (south)
Gaia DR2 5201378641555926784	10 55 59.69	-77 24 40.1	10.778	0.79	M0	3770 \pm 62	0.583 ^{+0.009} _{-0.002}	1.1 ^{+0.3} _{-0.0}	1.8 ^{+0.2} _{-0.1}	Cha I (south)
Gaia DR2 5201536661993294720	10 56 16.28	-76 30 53.1	12.542 \pm 0.024	0.00	M5.6	2900 \pm 100	0.049 ^{+0.002} _{-0.002}	1.1 ^{+1.5} _{-0.0}		Cha I (south)
Gaia DR2 5201388292344009984	10 56 30.28	-77 11 39.4	9.969 \pm 0.024	0.23	M0.5	3700 \pm 62	0.706 ^{+0.025} _{-0.023}		1.4 ^{+0.2} _{-0.2}	Cha I (south)
Gaia DR2 5201191037382571904	10 57 53.66	-77 24 49.7	11.615 \pm 0.023	0.34	M4	3160 \pm 120	0.146 ^{+0.007} _{-0.007}	1.4 ^{+0.5} _{-0.0}	2.9 ^{+0.5} _{-0.5}	Cha I (south)
Gaia DR2 5201387776948008320	10 58 05.86	-77 11 50.1	13.405 \pm 0.028	0.45	M5.25	2988 \pm 100	0.034 ^{+0.008} _{-0.002}	3.4 ^{+1.4} _{-0.0}	4.0 ^{+0.7} _{-0.0}	Cha I (south)
Gaia DR2 5201196599363180928	10 59 00.95	-77 22 40.9	10.135 \pm 0.023	0.34	K8	3940 \pm 22	0.741 ^{+0.028} _{-0.026}	1.3 ^{+0.2} _{-0.2}	2.0 ^{+0.3} _{-0.1}	Cha I (south)
Gaia DR2 5201226389256838528	10 59 06.87	-77 01 40.3	8.462 \pm 0.032	0.00	K2	4760 \pm 92	3.159 ^{+0.151} _{-0.141}		2.6 ^{+0.7} _{-0.7}	Cha I (south)
Gaia DR2 5201553704423697792	11 00 40.14	-76 19 28.0	11.859 \pm 0.026	0.20	M3.75	3210 \pm 120	0.111 ^{+0.005} _{-0.005}	2.0 ^{+1.3} _{-0.6}	3.7 ^{+1.0} _{-0.7}	Cha I (north)
Gaia DR2 5201194816953813504	11 01 13.58	-77 22 38.7	13.064 \pm 0.024	0.27	M5.25	2988 \pm 100	0.040 ^{+0.002} _{-0.003}	2.9 ^{+1.3} _{-0.0}	4.0 ^{+2.1} _{-0.0}	Cha I (south)
Gaia DR2 5201185574182015744	11 01 19.09	-77 32 38.7	13.096 \pm 0.033	0.45	M7.25	2630 \pm 58	0.040 ^{+0.003} _{-0.003}			Cha I (south)
Gaia DR2 5201218864474119808	11 01 31.93	-77 18 25.0	14.631 \pm 0.039	0.00	M8	2570 \pm 50	0.007 ^{+0.001} _{-0.000}			Cha I (south)
Gaia DR2 5225599096011296640	11 02 19.17	-75 36 57.6	12.131 \pm 0.027	0.27	M4.5	3020 \pm 120	0.088 ^{+0.004} _{-0.004}	1.5 ^{+1.0} _{-0.0}	3.2 ^{+0.8} _{-0.0}	Cha I (north)
Gaia DR2 5225743475632752128	11 02 26.01	-75 02 40.7	11.761 \pm 0.026	0.14	M4.75	2950 \pm 100	0.098 ^{+0.005} _{-0.004}		1.8 ^{+1.4} _{-0.0}	Cha I (north)
Gaia DR2 5201182413088266624	11 02 41.71	-77 24 24.6	12.804 \pm 0.026	0.72	M5	2880 \pm 100	0.067 ^{+0.003} _{-0.003}			Cha I (south)
Gaia DR2 5201206048291386880	11 02 54.91	-77 21 50.8	11.565 \pm 0.026	0.00	M4.5	3020 \pm 120	0.105 ^{+0.004} _{-0.004}	1.1 ^{+0.8} _{-0.0}	2.8 ^{+0.7} _{-0.0}	Cha I (south)
Gaia DR2 5201181313576638208	11 03 41.74	-77 26 52.1	12.997 \pm 0.024	0.61	M5.5	2925 \pm 100	0.057 ^{+0.003} _{-0.003}	1.4 ^{+1.2} _{-0.0}	0.5 ^{+4.0} _{-0.0}	Cha I (south)
Gaia DR2 5201206361825924992	11 03 47.54	-77 19 56.5	11.313 \pm 0.023	0.68	M5	2880 \pm 100	0.260 ^{+0.010} _{-0.011}			Cha I (north)
Gaia DR2 5201335481425778560	11 04 04.14	-76 39 33.0	12.953 \pm 0.023	0.74	M4.25	3090 \pm 120	0.063 ^{+0.003} _{-0.003}	2.7 ^{+1.7} _{-1.1}	4.6 ^{+1.4} _{-1.6}	Cha I (south)

Notes. We provide for each star the Gaia-DR2 identifier and position, J -band photometry and extinction in this band, spectral type, effective temperature, bolometric luminosity derived in this study, ages estimates inferred from the [Baraffe et al. \(2015, BHAC15\)](#) and [Siess et al. \(2000, SDF00\)](#) models, and the subgroup to which the star belongs. We used the spectral types and extinctions compiled by [Esplin et al. \(2017\)](#) and [Spezzi et al. \(2008\)](#) for Cha I and Cha II stars, respectively.